

Synthesis and import of GDP-L-fucose into the Golgi affect plant–water relations

Cezary Waszczak¹ , Dmitry Yarmolinsky² , Marina Leal Gavarrón¹ , Triin Vahisalu¹ , Maija Sierla¹ , Olena Zamora² , Ross Carter³ , Tuomas Puukko¹ , Nina Sipari^{1,4} , Airi Lamminmäki¹ , Jörg Durner⁵ , Dieter Ernst⁵ , J. Barbro Winkler⁶ , Lars Paulin⁷ , Petri Auvinen⁷ , Andrew J. Fleming⁸ , Mats X. Andersson⁹ , Hannes Kollist²  and Jaakko Kangasjärvi¹ 

¹Organismal and Evolutionary Biology Research Programme, Faculty of Biological and Environmental Sciences, Viikki Plant Science Centre, University of Helsinki, FI-00014, Helsinki, Finland; ²Institute of Technology, University of Tartu, 50411, Tartu, Estonia; ³Sainsbury Laboratory, University of Cambridge, CB2 1LR, Cambridge, UK; ⁴Viikki Metabolomics Unit, Faculty of Biological and Environmental Sciences, University of Helsinki, FI-00014, Helsinki, Finland; ⁵Institute of Biochemical Plant Pathology, Helmholtz Zentrum München, German Research Center for Environmental Health, 85764, Neuherberg, Germany; ⁶Research Unit Environmental Simulation, Helmholtz Zentrum München, German Research Center for Environmental Health, 85764, Neuherberg, Germany; ⁷Institute of Biotechnology, University of Helsinki, FI-00014, Helsinki, Finland; ⁸School of Biosciences, University of Sheffield, S10 2TN, Sheffield, UK; ⁹Department of Biological and Environmental Sciences, University of Gothenburg, SE-405 30, Gothenburg, Sweden

Summary

Authors for correspondence:

Cezary Waszczak

Email: cezary.waszczak@helsinki.fi

Jaakko Kangasjärvi

Email: jaakko.kangasjarvi@helsinki.fi

Received: 18 April 2023

Accepted: 13 October 2023

New Phytologist (2023)

doi: 10.1111/nph.19378

Key words: cell wall, fucose metabolism, plant–water relations, rhamnogalacturonan II, stomata.

- Land plants evolved multiple adaptations to restrict transpiration. However, the underlying molecular mechanisms are not sufficiently understood.
- We used an ozone-sensitivity forward genetics approach to identify *Arabidopsis thaliana* mutants impaired in gas exchange regulation.
- High water loss from detached leaves and impaired decrease of leaf conductance in response to multiple stomata-closing stimuli were identified in a mutant of MURUS1 (MUR1), an enzyme required for GDP-L-fucose biosynthesis. High water loss observed in *mur1* was independent from stomatal movements and instead could be linked to metabolic defects. Plants defective in import of GDP-L-Fuc into the Golgi apparatus phenocopied the high water loss of *mur1* mutants, linking this phenotype to Golgi-localized fucosylation events. However, impaired fucosylation of xyloglucan, N-linked glycans, and arabinogalactan proteins did not explain the aberrant water loss of *mur1* mutants.
- Partial reversion of *mur1* water loss phenotype by borate supplementation and high water loss observed in boron uptake mutants link *mur1* gas exchange phenotypes to pleiotropic consequences of L-fucose and boron deficiency, which in turn affect mechanical and morphological properties of stomatal complexes and whole-plant physiology. Our work emphasizes the impact of fucose metabolism and boron uptake on plant–water relations.

Introduction

The leaves and stems of terrestrial plants are covered with a hydrophobic layer called the cuticle, which directs the majority of plant gas exchange toward stomata. Stomata are epidermal pores surrounded by pairs of guard cells. Guard cells respond to multiple environmental factors, for example light, leaf internal CO₂ concentration, drought, air humidity, pathogens and air pollutants such as ozone (O₃), to optimize CO₂ uptake and control water loss, or prevent the entry of pathogens into the leaf tissue. Perception of stomata-closing stimuli initiates a complex series of guard cell signaling events ultimately leading to guard cell plasma membrane depolarization and activation of K⁺_{out} channels (Merlot *et al.*, 2007; Hedrich, 2012; Sierla *et al.*, 2016; Yamauchi *et al.*, 2016; Pei *et al.*, 2022). The release of ions into the apoplast leads to a decrease in osmotic pressure inside the

guard cells, which provokes an efflux of H₂O from the guard cell cytoplasm and vacuole. The consequent drop in guard cell turgor pressure results in closure of stomatal pores (Franks *et al.*, 1998).

To allow the volume and pressure changes, guard cell walls exhibit a high degree of elasticity, which is determined by specialized wall composition (Amsbury *et al.*, 2016; Merced & Renzaglia, 2018; Carroll *et al.*, 2022). Plants deficient in pectin modifications exhibit defects in stomatal movements, which suggests that the status of pectin crosslinking determines the mechanical properties of guard cell walls (Amsbury *et al.*, 2016; Chen *et al.*, 2021). Furthermore, the cellulose microfibrils that fan out radially from the pore (see Shtein *et al.*, 2017 for a recent visualization) provide a hoop reinforcement that limits the increase in guard cell radius and promotes guard cell elongation during the stomatal opening (Woolfenden *et al.*, 2017). Moreover, the stiffness of guard cell walls is not uniform; the most

rigid areas are localized at the guard cell poles and ventral walls directly surrounding the pore (Carter *et al.*, 2017). Taken together, next to guard cell signaling, the mechanics of the guard cell walls has a profound role in the execution of stomatal movements (Woolfenden *et al.*, 2018; Yi *et al.*, 2019). Importantly, the expansion and flexing of guard cells need to overcome the turgor pressure of the neighboring epidermal cells. Recently, Nieves-Cordones *et al.* (2022) found that decreased pavement cell turgor, observed in mutants of K⁺ RECTIFYING CHANNEL 1 (KC1) channel subunit due to decreased K⁺ accumulation, results in wider stomatal apertures, higher stomatal conductance, and elevated loss of water from detached leaves. These results demonstrate that the counter pressure exerted onto the guard cells by the pavement cells is required for stomatal closure.

The synthesis of cell wall glycan polymers relies on the availability of nucleotide sugars that constitute the activated precursor forms serving as a donor of sugar moieties (Bar-Peled & O'Neill, 2011). The importance of nucleotide sugar synthesis and transport can be exemplified by the requirement of GDP-L-fucose for proper growth and development. The synthesis of GDP-L-Fuc is initiated by GDP-D-mannose 4,6-dehydratases (GMD1) and MURUS1 (MUR1/GMD2) that catalyze the conversion of GDP-D-mannose to GDP-4-keto-6-deoxy-D-mannose (Supporting Information Fig. S1; Bonin *et al.*, 1997, 2003).

In *mur1* leaves the level of L-Fuc is reduced by *c.* 98% (Reiter *et al.*, 1993). Plants lacking MUR1 exhibit abnormal development (Reiter *et al.*, 1993; Van Hengel & Roberts, 2002; Voxeur *et al.*, 2017) and stress responses (Panter *et al.*, 2019; Zhang *et al.*, 2019). The product of the MUR1-catalyzed reaction serves as a substrate for the GDP-4-keto-6-deoxymannose-3,5-epimerase-4-reductases GER1 (Bonin & Reiter, 2000; Nakayama *et al.*, 2003) and GER2 (Rhomberg *et al.*, 2006) that complete the synthesis of GDP-L-Fuc (Fig. S1). Additionally, the L-fucose salvage pathway involving a single bifunctional enzyme L-FUCO-KINASE/GDP-L-FUCOSE PYROPHOSPHORYLASE (FKGP) recycles L-Fuc, released during, for example cell wall remodeling, back to GDP-L-Fuc (Kotake *et al.*, 2008).

Following synthesis in the cytoplasm, GDP-L-Fuc is transported into the Golgi lumen by the GDP-FUCOSE TRANSPORTER1 (GFT1; Rautengarten *et al.*, 2016) where it serves as a substrate for fucosyltransferases (FUTs) that fucosylate molecules such as xyloglucan (FUT1/MUR2, Perrin *et al.*, 1999; Vanzin *et al.*, 2002), arabinogalactan proteins (FUT4, FUT6; Wu *et al.*, 2010; Liang *et al.*, 2013; Tryfona *et al.*, 2014), and N-linked glycans (FUT11/FUCTA, FUT12/FUCTB, FUT13/FUCTC; Leonard *et al.*, 2002; Strasser *et al.*, 2004). Moreover, L-Fuc is found in rhamnogalacturonan II (RG-II), and the dwarf phenotype of *mur1* mutants has been previously attributed to deficiency in boron-dependent dimerization of this pectin (O'Neill *et al.*, 2001). In *mur1*, RG-II L-Fuc residues are replaced by L-galactose (Zablackis *et al.*, 1996) which leads to an *c.* 50% decrease in RG-II dimer formation (O'Neill *et al.*, 2001) caused by RG-II chain A truncation (Pabst *et al.*, 2013).

To understand the processes controlling plant gas exchange, ozone (O₃) can be used as an apoplastic ROS donor to stimulate stomatal closure (Overmyer *et al.*, 2000; Kollist *et al.*, 2007; Vahisalu *et al.*, 2010). Plants deficient in O₃-induced stomatal closure, or those in which epidermal integrity is affected, receive high doses of O₃ that triggers the formation of visible hypersensitive response-like lesions. Here, we describe the identification of the MUR1 mutant from an O₃-sensitivity screen and show that synthesis and import of GDP-L-fucose into the Golgi play an important role in regulating plant gas exchange. Our results are consistent with the hypothesis that the gas exchange phenotypes observed in *mur1* mutants are independent from stomatal movements and we propose that changes in stomatal morphology, and likely also elevated water vapor permeability of mesophyll/epidermal barriers, contribute to the high rates of water loss observed in *mur1* mutants.

Materials and Methods

See Methods S1 for detailed description of methods used in this study.

Plant material and growth conditions

Mutant *T7-9/mur1-10* was identified from the genetic screen involving the use of environmental simulation chambers (ExpoSCREEN, Helmholtz Zentrum München) as described earlier (Sierla *et al.*, 2018). Aside from mutant *T7-9/mur1-10* that was in pGC1:YC3.6 genetic background and *qua1-1* (Ws-4 background), all lines used in this study were in Col-0 background. See Dataset S1 for description of all *Arabidopsis thaliana* (L.) Heynh. lines used in this study. *E.coli* and *Agrobacterium tumefaciens* strains carrying the hpGFT1 construct (Rautengarten *et al.*, 2016) were obtained from Joshua L. Heazlewood. T1 hpGFT1 plants were generated as described before (Rautengarten *et al.*, 2016). Two-wk-old T1 plants were transplanted to soil and grown for additional 3 wk as described below. The same selection procedure has been applied to select for empty vector lines. Other control lines were grown in parallel, except the selection antibiotic was not included in the growth medium.

Unless specified otherwise, seeds were suspended in 0.1% agarose solution, vernalized in the dark for 2 d at 4°C and sown on a 1 : 1 mixture of peat and vermiculite. Plants were grown in controlled growth rooms under 12 h : 12 h, light (200 μmol m⁻² s⁻¹) : dark cycle, 22°C : 18°C (day : night), 60% : 70% relative humidity. If not otherwise specified, experiments were performed on 3.5-wk-old soil-grown plants.

Water loss assay

Two middle-aged leaves of 3.5-wk-old soil-grown plants were cut and dried abaxial side up at room temperature for 2 h, unless specified otherwise. Mass of leaves was determined before and after drying, and water loss was calculated as percentage of initial fresh weight loss.

Ion leakage assay

The ion leakage was performed by collecting whole rosettes of 3.5-wk-old soil-grown plants into 15 ml of MilliQ water and measuring the conductance of the solution after 6 and 18 h using conductivity meter (FiveEasy FE30; Mettler-Toledo, Columbus, OH, USA). Later, samples were frozen (-20°C) and thawed at room temperature, and the final conductance measurement was performed. Ion leakage was calculated as (%) of conductance recorded after thawing.

Toluidine blue dye-exclusion assay

Toluidine blue dye-exclusion assays (Tanaka *et al.*, 2004) were performed on middle-aged leaves of 3.5-wk-old soil-grown plants. Two 4 μl drops of staining solution (0.05% w/v toluidine blue, 0.01% v/v Tween 20) were applied to adaxial side of the leaves, one on each side of the central vein. Subsequently, plants were covered with transparent lids to maintain high humidity. After 2 h, leaves were abundantly sprayed with water to remove the staining solution. After water has evaporated, leaves were detached and photographed with Nikon D5100 camera equipped with AF-S Micro Nikkor 40 mm 1 : 2.8G objective (Nikon, Tokyo, Japan).

Infrared imaging

Three middle-aged leaves were detached and imaged with Optris PI 450 infrared camera (Optris GmbH, Berlin, Germany) equipped with 10 mm lens. Images were captured at 2-s interval, and leaf temperatures were extracted with the use of OPTIRIS PI CONNECT (v.2.9.2147.0) software.

Metabolomics

The GDP-L-fucose was quantified with UPLC-6500+ QTRAP/MS system (Sciex, Redwood City, CA, USA) in negative (ESI-) multiple reaction monitoring (MRM) mode.

Waxes were extracted by individually dipping 5–6 middle-aged leaves of 5-wk-old soil-grown plants into chloroform for 30 s. The samples were dried under a stream of nitrogen, and analysis of wax monomers was performed as described previously (Fahlberg *et al.*, 2019).

Approximately 0.5 g of leaf material collected from 4.5-wk-old soil-grown plants was processed as described earlier (Jenkin & Molina, 2015). Levels of individual cutin components were analyzed by GC-MS.

Gas exchange analysis

The gas exchange experiments were performed with multicuvette gas exchange system (PlantInvent Ltd, Tartu, Estonia) as described previously (Sierla *et al.*, 2018). Leaf conductance was calculated as transpiration divided by the difference in molar concentrations of water vapor inside the leaf and in the ambient air in the measuring chamber (Kollist *et al.*, 2007). To characterize minimal leaf conductance, plants were incubated for at least 1 h in darkness at

800 $\mu\text{l l}^{-1}$ CO_2 to induce maximal stomatal closure. After stabilization of leaf conductance, rosettes were detached from the roots with a razor blade and leaf conductance measurements were continued for 64 min. The stabilized new levels of leaf conductance were defined as minimal leaf conductance.

Mapping by next-generation sequencing

Rosettes were harvested in bulk and used for preparation of nuclear DNA. The nuclear DNA-enriched sample was sequenced (2×150 bp) using NextSeq 500 sequencer (Illumina, San Diego, CA, USA) to an *c.* 50-fold genome coverage at DNA Sequencing and Genomics Laboratory, Institute of Biotechnology, University of Helsinki. Data were analyzed according to the procedure described earlier (Sun & Schneeberger, 2015).

Expression analysis by qPCR

For gene expression analysis of T-DNA insertion mutants, plants were grown vertically on half-strength Murashige & Skoog medium (Duchefa Biochemie, Haarlem, the Netherlands) in controlled growth chambers (model MLR-350; Sanyo, Osaka, Japan) under 12 h : 12 h, light ($130\text{--}160 \mu\text{mol m}^{-2} \text{s}^{-1}$) : dark cycle, 22°C : 18°C (day : night). For every biological replicate (three in total), *c.* 10 whole 2-wk-old plants were pooled, frozen, and ground in liquid nitrogen. For analysis of *GFT1* transcript level, whole rosettes of T1 hp*GFT1* plants (minus two middle-aged leaves that were used for water loss assay) were frozen in liquid nitrogen and ground with a mortar and pestle. RNA isolation, cDNA synthesis, qPCR, and data analysis were performed as described previously (Xu *et al.*, 2015).

Stomatal morphology

Cotyledons (one cotyledon per plant, four–six plants per line per biological replicate, three biological replicates) were processed (see Methods S1), and serial images ($1800\times$ magnification, 10% overlap) were taken with Quanta FEG 250 (Thermo Fisher Scientific, Waltham, MA, USA) scanning electron microscope at the Electron Microscopy Unit, Institute of Biotechnology, University of Helsinki. Images were stitched in IMAGEJ (Schindelin *et al.*, 2012) implementing MIST plugin (Chalfoun *et al.*, 2017). For each cotyledon, from 1 to 2.5 mm^2 area was analyzed, containing 100–350 stomatal complexes. Stomatal morphology was assessed visually and assigned into one of the four categories: normal appearance, not determined, covered, and abnormally large/obstructed. The size of stomatal pores was determined with the use of the IMAGEJ.

For observation of stomata on abaxial side of true leaves *c.* 4 \times 4 mm fragments of middle-aged leaves were excised, mounted on aluminum stubs, and plunged into slush nitrogen. Samples were coated with 5 nm platinum in Quorum PP3010T Cryo-SEM preparation system, and SEM images were acquired with JEOL JIB-4700F Multi Beam System at the OtaNano-Nanomicroscopy Center, Aalto University. Five to six 0.2 mm^2 images per each leaf fragment were captured, and the stomatal density and morphology were assessed with the help of IMAGEJ.

Projected rosette area

Rosettes were photographed with Nikon D5100 camera equipped with AF-S Micro Nikkor 40 mm 1 : 2.8G objective (Nikon). The projected rosette area was determined with IMAGEJ.

Atomic force microscopy

For AFM experiments, seeds were stratified for 7 d at 4°C, then grown in a 3 : 1 compost : perlite mix. Growth conditions were as follows: light intensity 170 $\mu\text{mol m}^{-2} \text{s}^{-1}$, 12 h : 12 h, day : night, (21°C) : (17°C), 60% humidity. Leaves from *c.* 21-d-old plants were analyzed as described previously (Carter *et al.*, 2017). Dissected and plasmolyzed (0.55 M mannitol; minimum 45 min) leaf blocks (*c.* 5 × 5 mm square) were indented using a Nano Wizard 3 AFM (JPK Instruments, Berlin, Germany) mounted with a nominal 5 nm diameter pyramidal indenter (Windsor Scientific, Slough, UK) on a cantilever of nominal 45 N m⁻¹ stiffness. Cantilever stiffness was calibrated using the thermal tuning method available in the JPK controller software. Cantilever sensitivity was calibrated by performing indentation measurements on a glass slide and was repeated for each experiment.

For each leaf block, an area of 100 × 100 μm was indented by splitting the area into a grid of 128 × 128 indentations. Indentations were stopped when an indentation force of 1000 nN was reached, which corresponds to an indentation depth of between 100 and 1000 nm. Force indentation curves were analyzed with the JPKSPM Data Processing software (JPK Instruments; v.spm 5.0.69) using the following steps: Raw voltage values converted to force values using the calibrated cantilever sensitivity and stiffness, baseline corrected for offset and tilt, displacement offset corrected, indentation calculation, and material property calculation using a Hertzian indentation model to the approach curve. Use of the Hertzian model assumes an infinite homogenous elastic half space, which is clearly not the case for the leaf surface. For this reason, we report results as an apparent modulus (E_a). Retraction curves were discarded due to numerous complications with adhesion between the tip and sample surface.

Observation of dark-elongated hypocotyls by confocal microscopy

Seeds were stratified, surface-sterilized, and sown on agar-solidified (0.8% w/v) 1/2 MS (Duchefa Biochemie) supplemented with 0.5 g l⁻¹ MES pH 5.8 and 1% sucrose. Following 7 h exposure to light, plates were incubated vertically for 4 d in controlled growth chambers (MLR-350; Sanyo) at 23°C in darkness. Seedlings were stained with 0.2 mg ml⁻¹ propidium iodide (PI, Sigma-Aldrich) and imaged using Leica Stellaris 8 confocal microscope equipped with the Leica Application Suite X package. Propidium iodide (PI) excitation was performed using a 552 nm solid-state laser, and fluorescence was detected at 600–650 nm. Stacks of 1024 × 1024 pixels optical section were generated with a Z interval of 1 μm . 3D images were reconstructed using the Leica Application Suite LAS X 3D v.4.5.0. In every biological replicate (3 in total), 5–10 plants per line were imaged.

Measurement of stomatal apertures

Plants were sprayed with a solution containing 5 μM ABA (Duchefa), 0.012% (v/v) Silwet, and 0.05% (v/v) ethanol or mock solution. After 45 min, two middle-aged leaves per plant were detached and the abaxial side was immediately coated with Xantopren M Mucosa (Kulzer GmbH, Hanau, Germany). After 24 h, the molds were peeled off and coated with transparent nail polish. The nail polish imprints were imaged with the use of Leica DMLB microscope equipped with Leica 20× Fluotar objective. Two images per leaf were captured, one per each side of the central vein. Images were analyzed with IMAGEJ, and stomatal apertures were calculated as stomatal length : width ratio.

Results

Lack of MUR1 results in high rates of water loss

To identify novel regulators of plant gas exchange, we performed a multistep forward genetic screen based on O₃-sensitivity (Sierla *et al.*, 2018; Takahashi *et al.*, 2022). The screen was performed on EMS-mutagenized pGC1:Yellow Cameleon 3.6 (YC3.6, Yang *et al.*, 2008) line. Aside from O₃-sensitivity, the water loss assay, also known as ‘mass loss of detached leaves, MLD’ (Duursma *et al.*, 2019), was used in this screen as a simple indicator of minimal leaf conductance (g_{min}). The g_{min} is a sum of cuticular conductance (g_{cuti}) and residual stomatal conductance observed after the detachment of leaves (minimal stomatal conductance, $g_{\text{s-min}}$). Elevated water loss can be observed in mutants impaired in stomatal closure (Vahisalu *et al.*, 2008; Hōrak *et al.*, 2016; Sierla *et al.*, 2018) or cuticular/epidermal integrity, for example those deficient in cutin biosynthesis (Bessire *et al.*, 2007; Jakobson *et al.*, 2016) or epidermal cell adhesion (Bouton *et al.*, 2002; Mouille *et al.*, 2007).

From this screen, we isolated mutant *T7-9* that exhibited high water loss from detached leaves (Fig. 1a) and altered gas exchange dynamics in response to O₃, high CO₂ concentration, ABA, and darkness (Fig. S2). To identify the *T7-9* causative mutation, we applied the SHOREmap backcross pipeline (Hartwig *et al.*, 2012). Approximately 21% of the BC_{1F2} plants (123 out of 593) exhibited increased water loss, indicating that the trait was determined by a single recessive mutation.

Screening of the mutant lines for the five candidate genes (Table S1) revealed that three independent mutant lines: *mur1-1*, *mur1-2* (Reiter *et al.*, 1993; Bonin *et al.*, 1997) and *mur1-9* (SALK_057153, Fig. S3), carrying mutations within *AT3G51160* (Fig. 1b), exhibited highly elevated water loss (Fig. 1c), while mutant lines for the remaining candidate genes did not (Fig. S4). Monitoring of leaf temperature during the water loss experiment revealed that, in Col-0, detachment of leaves significantly increased leaf temperature while the temperature of *mur1* leaves closely resembled that of *ghr1-3* indicating comparable rates of g_{min} (Fig. S5).

AT3G51160 encodes GDP-mannose-4,6-dehydratase MURUS1 (GMD2, MUR1), which catalyzes the first step in *de novo* biosynthesis of GDP-L-Fucose (Fig. S1; Bonin *et al.*, 1997).

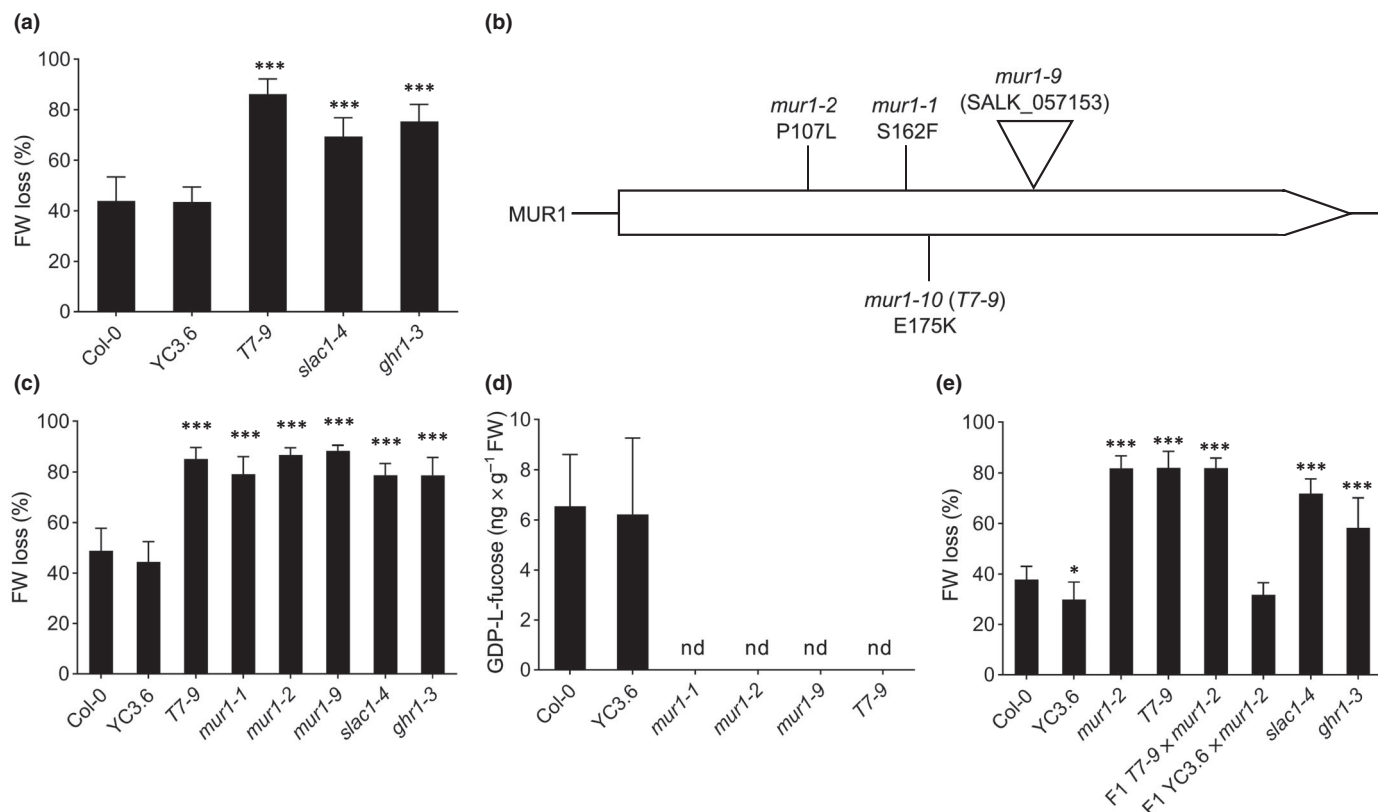


Fig. 1 Mapping of *Arabidopsis thaliana* T7-9 mutant. (a) Leaf fresh weight loss of T7-9 and control lines (YC3.6, Col-0, *slac1-4*, and *ghr1-3*) recorded after 2 h. Data bars represent means \pm SD ($n = 12$ plants). (b) Positions of mutations in *mur1* mutants used in this study. (c) Leaf fresh weight loss of T7-9, independent *mur1* mutants (*mur1-1*, *mur1-2*, and *mur1-9*) and control lines (YC3.6, Col-0, *slac1-4*, and *ghr1-3*) recorded after 2 h. Data bars represent means \pm SD ($n = 12$ plants). (a, c) Asterisks denote statistical differences (***, $P < 0.001$) to respective control lines (Col-0 or YC3.6) according to one-way ANOVA followed by Šidák's *post hoc* test. (d) GDP-L-fucose content in T7-9, *mur1* mutants and respective control lines measured by UPLC-MS. Data bars represent means \pm SD ($n = 4-5$ plants); nd, not detected; FW, fresh weight. (e) Leaf fresh weight loss of T7-9, *mur1-2*, F1 T7-9 \times *mur1-2*, and F1 YC3.6 \times *mur1-2* and control lines recorded after 2 h. Data bars represent means \pm SD ($n = 9-12$ plants). Asterisks denote statistical differences (*, $P < 0.05$; ***, $P < 0.001$) to Col-0 according to one-way ANOVA followed by Dunnett's *post hoc* test. (a, c, e) Experiments were repeated three times with similar results. Results of the representative experiments are shown.

Therefore, we investigated the level of GDP-L-Fuc in the T7-9 mutant. Like in other *mur1* mutants, we were not able to detect this metabolite in T7-9, suggesting complete loss of MUR1 enzymatic activity (Fig. 1d). Finally, an allelism test between T7-9 and *mur1-2* mutant revealed lack of complementation, confirming that the T7-9 MUR1 E175K mutation (hereafter referred to as *mur1-10*) conferred its high water loss (Fig. 1e).

Impaired import of GDP-L-fucose into the Golgi apparatus results in high rates of water loss

Following the identification of *mur1* mutant, we set out to investigate the water loss of mutants impaired in the GDP-L-Fuc salvage pathway and import into the Golgi. The water loss of *fkcp* mutants (*fkcp-1*, *fkcp-2*, Kotake *et al.*, 2008) was similar to that of Col-0 (Fig. S6), indicating that the L-fucose salvage pathway has little impact on plant gas exchange. Further, we focused on characterization of the GDP-L-Fuc transporter GFT1. Loss-of-function mutants of GFT1 are not viable; therefore, we utilized the hairpin RNAi strategy used earlier by Rautengarten *et al.* (2016) to generate GFT1 knockdown plants (*hpGFT1*). A total of 66 independent *hpGFT1* T1 plants were selected and transplanted to soil. As

observed before (Rautengarten *et al.*, 2016), the *hpGFT1* plants exhibited varying growth phenotypes, that is reduced projected rosette area, short petioles and wavy leaves (Fig. S7a).

For each of the T1 *hpGFT1* plant that survived in soil (64 plants), we measured the projected rosette area, loss of water from detached leaves, and the *GFT1* transcript level (58 plants). The *hpGFT1* T1 plants exhibited varying water loss (Fig. 2a) and residual *GFT1* transcript level (Fig. 2b) and displayed a clear negative correlation between these two traits (Figs 2c, S7b). Similarly, the projected rosette area was also negatively correlated with the water loss (Fig. S7c). The majority of *hpGFT1* plants with *GFT1* transcript level lower than 10% of that observed in the empty vector control displayed water loss comparable to that of *mur1* mutants (Fig. 2c). Thus, we conclude that not just the synthesis but also the import of GDP-L-Fuc into the Golgi lumen is required for normal plant gas exchange.

MUR1 is required for regulation of plant gas exchange

To further characterize the gas exchange dynamics in *mur1* mutants, we subjected them to a variety of treatments provoking stomatal movements and followed time-resolved whole-rosette

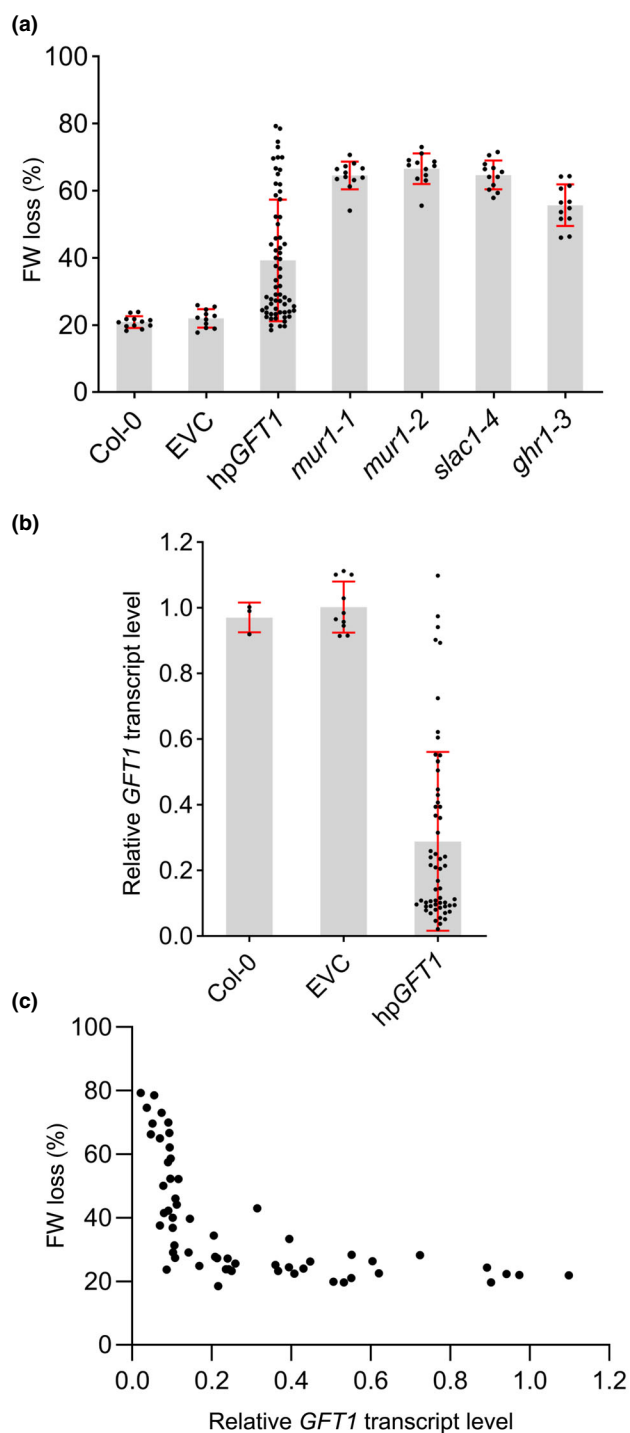


Fig. 2 Effect of impaired import of GDP-L-Fuc into Golgi on the water loss. (a) Leaf fresh weight loss of 64 independent *Arabidopsis thaliana* hpGFT1 T1 plants (hp, hairpin), and control lines (Col-0, EVC – empty vector control, *mur1-1*, *mur1-2*, *slac1-4*, and *ghr1-3*), recorded after 2 h. Data points represented values obtained for separate plants. Data bars represent means \pm SD (for control lines $n = 11$ – 12 plants). (b) Variability in *GFT1* transcript level observed in 58 independent *A. thaliana* hpGFT1 T1 plants. Data points represent values obtained for separate plants. Data bars represent means \pm SD; Col-0 $n = 3$ plants, EVC $n = 10$ plants. (c) Residual *GFT1* transcript level and fresh weight loss observed in 58 independent *A. thaliana* hpGFT1 T1 plants. Each dot represents values obtained for an independent hpGFT1 T1 plant.

transpiration and leaf conductance (Kollist *et al.*, 2007; Jakobson *et al.*, 2016). Gas exchange measurements were performed for *mur1-1* and *mur1-2* mutants (Reiter *et al.*, 1993; Bonin *et al.*, 1997) using *ghr1-3* (Sierla *et al.*, 2018) and *ht1-2* (Hashimoto *et al.*, 2006) as nonresponsive controls in closure and opening assays, respectively.

As observed earlier in *T7-9* (Fig. S2) in response to a 3-min O_3 pulse, plants lacking MUR1 displayed the rapid transient decrease in leaf conductance (Figs 3a,b, S8a, S9a) with lower magnitude than Col-0 plants whereas O_3 response was not present in *ghr1-3* plants (Sierla *et al.*, 2018).

Similarly, a decreased response upon treatment with elevated CO_2 concentration ($800 \mu l l^{-1}$), 5 μM ABA spray or application of darkness during the light period was observed in *mur1* mutants (Figs 3c–h, S8b–d, S9b–d; Dataset S2). During diurnal light/dark cycles, the transition to darkness induced a rapid drop in transpiration and leaf conductance of Col-0 plants while *mur1* mutants exhibited a much less pronounced response (Figs S8e, S9e).

The stimuli provoking stomatal opening, such as exposure to low CO_2 concentration ($400 \rightarrow 100 \mu l l^{-1}$) or increase in light intensity ($150 \rightarrow 500 \mu mol m^{-2} s^{-1}$), did not show any differences between *mur1* mutants and the wild-type (WT; Fig. S10).

To estimate minimal leaf conductance, we treated *mur1* and Col-0 plants with a combination of stomata-closing stimuli (elevated CO_2 concentration and darkness) for 1 h, after which the rosettes were separated from roots to ensure maximal stomatal closure. Such treatment triggered reduction of leaf conductance in all tested lines; however, in *mur1* mutants the leaf conductance stabilized at values two times higher than in Col-0 (Fig. S11). Taken together, our data indicate that stomata of *mur1* plants responded to O_3 , high CO_2 concentration, ABA, and darkness; however, with no regard to the stimulus, the post-treatment leaf conductance always remained higher than that of the WT plants indicating general impairment in gas exchange regulation.

MUR1 is involved in stomatal development

To assess stomatal development, we performed scanning electron microscopy-based examination of abaxial epidermis of *mur1-1* and *mur1-2* cotyledons. No consistent phenotype related to stomatal density was observed in *mur1* mutants. The stomatal density in *mur1-2* mutant was higher than in *mur1-1*, which had a similar stomatal density to Col-0 (Fig. 4a). The average size of stomatal pores was moderately increased in the *mur1-1* mutant, while in *mur1-2* there were no significant differences compared with Col-0 (Fig. 4b). Notably, in cotyledons of both mutants we sporadically observed abnormally big stomatal complexes (4–5% of total stomata, Fig. S12a) that were irregular in shape and often visibly obstructed (Fig. S12b). Moreover, a fraction of *mur1* stomata exhibited aberrant structure of the outer cuticular ledge (OCL). In the most severe cases (5–10% of stomata, Fig. S12a), stomatal pores appeared covered with cuticle (Fig. 4c).

Examination of middle-aged rosette leaves, that is leaves which were used for water loss assay, by means of cryo-SEM revealed similar phenotypes (Dataset S3a), except no abnormally big/

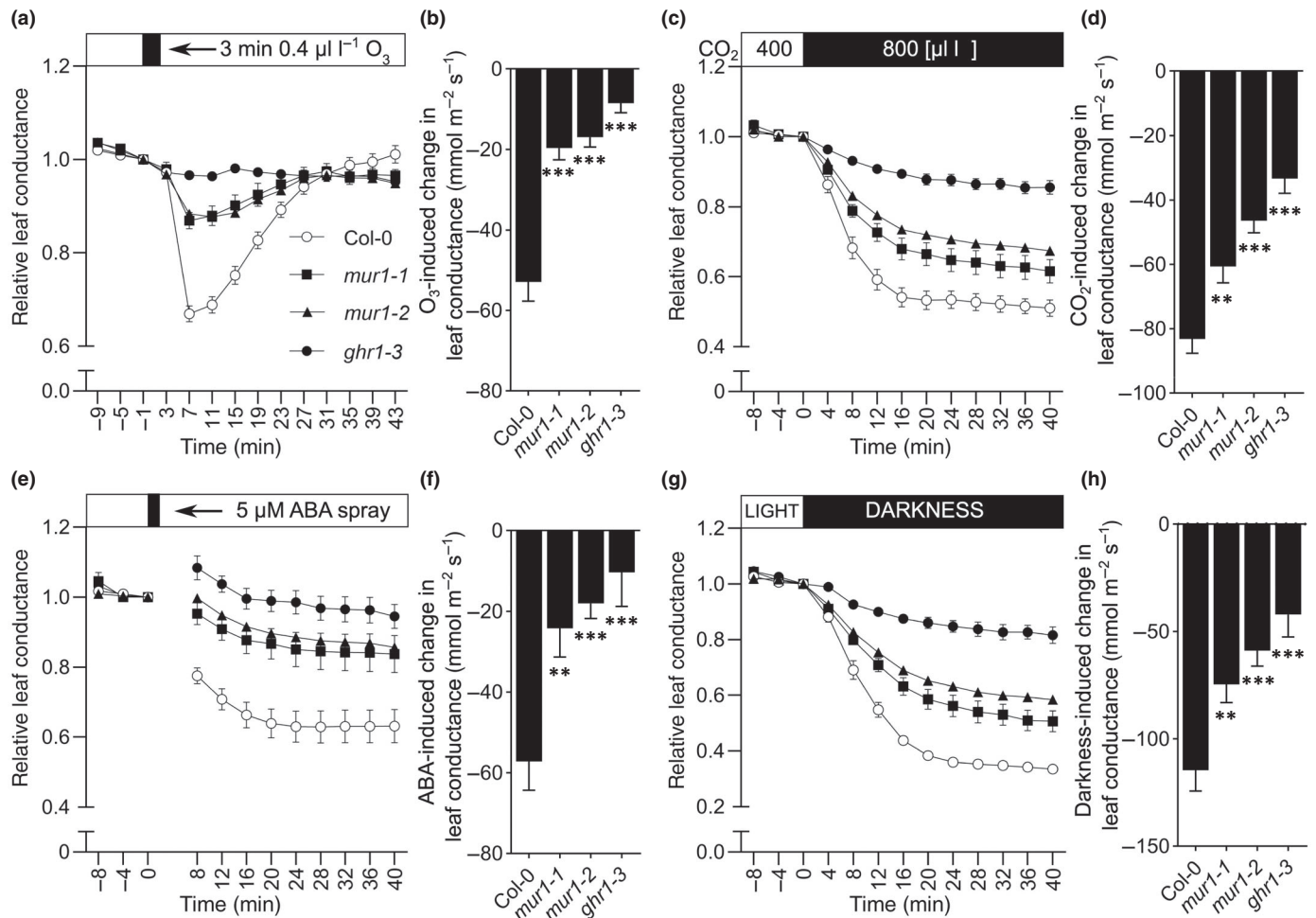


Fig. 3 Characterization of *mur1* gas exchange dynamics. (a–h) Leaf conductance responses of *Arabidopsis thaliana* *mur1* mutants to stomata-closing stimuli. ABA, abscisic acid. Relative and absolute values were calculated from the data presented in Supporting Information Fig. S8. (a, c, e, g) Time course of relative leaf conductance (normalized to the last time point before the treatment) of 3- to 4-wk-old *mur1-1*, Col-0, and *ghr1-3* plants in response to (a) O₃ pulse, (c) elevated CO₂, (e) ABA spray, and (g) darkness. The indicated treatments were applied at *t* = 0, and whole-rosette leaf conductance was recorded. Data points represent means ± SE; *n* = 7–10 (a), 10–12 (c), 9–11 (e), 6–11 (g) plants analyzed in two (a, e, g) or three (c) independent experiments. (b, d, f, h) Changes in leaf conductance of Col-0, *mur1-1*, *mur1-2*, and *ghr1-3* in response to (b) O₃ pulse, (d) elevated CO₂, (f) ABA spray, and (h) darkness. Values were calculated by subtracting the initial leaf conductance at *t* = 0 (d, f, h) or *t* = -1 (b) from the leaf conductance at *t* = 7 min, (d, f, h) *t* = 40 min. Data bars represent means ± SE; *n* = 7–10 (b), 10–12 (d), 9–11 (f), 6–11 (h) plants. Asterisks denote statistical differences to Col-0 (**, *P* < 0.01; ***, *P* < 0.001) according to one-way ANOVA followed by Dunnett's *post hoc* test.

obstructed stomata were detected. The stomatal density was elevated in *mur1-2* (Fig. 4d), and in both mutants, c. 10% of stomata were covered with OCLs (Fig. 4e). Overall, despite the differences in stomata size and morphology, in the majority of experiments, the daytime whole-rosette leaf conductance of *mur1* mutants did not differ significantly from that of the WT plants (Figs S8E, S13). We however observed that the leaf conductance of *mur1-2* tended to be smaller than that of Col-0 (Fig. S13). This difference is probably associated with the higher frequency of 'covered' stomata observed in this mutant (Fig. 4e).

High rate of water loss is independent of stomatal movements in *mur1* mutants

A series of experiments was performed to elucidate whether altered plant gas exchange dynamics observed in *mur1* mutants is

related to impaired guard cell signaling or stomatal movements. We crossed *mur1-1* and *mur1-2* to *slac1-4* (Vahisalu *et al.*, 2008), *aba2-11* (González-Guzmán *et al.*, 2002), *ost1-3* (Yoshida *et al.*, 2002), and *ghr1-3* (Sierla *et al.*, 2018) and assayed the stomatal function of the double mutants via water loss assay. In every double mutant, an additive effect of combining two mutations could be observed (Fig. 5a), indicating that the phenotypes observed in *mur1* plants were independent from the canonical guard cell signaling pathways.

Because of the additive effects and the previously documented role of MUR1 in cell wall development, we investigated the mechanical properties of *mur1* guard cell walls with atomic force microscopy (Carter *et al.*, 2017). The patterning of the apparent modulus (*E_a*) in the stomatal complexes of *mur1* mutants was comparable to that of the control lines. However, comparison of the absolute *E_a* values derived from the AFM scans indicated that

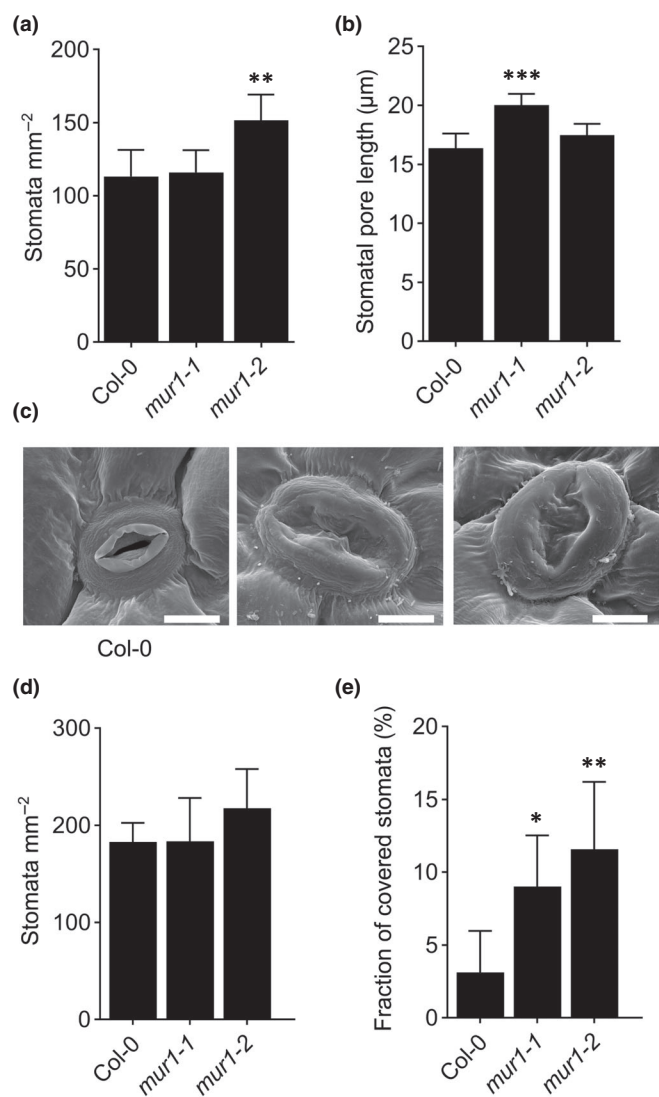


Fig. 4 Stomatal development in *Arabidopsis thaliana* *mur1* mutants. (a) Stomatal density and (b) mean stomatal pore length on abaxial side of 3-wk-old cotyledons of Col-0, *mur1-1*, and *mur1-2*. (a, b) Data bars represent means \pm SD ($n = 4-6$ cotyledons, 1 cotyledon per plant). Asterisks denote statistical differences (**, $P < 0.01$; ***, $P < 0.001$) to Col-0 according to one-way ANOVA followed by Dunnett's *post hoc* test. Experiments were performed three times with similar results. (c) Representative scanning electron microscopy images of 'covered' stomata observed on abaxial side of 3-wk-old cotyledons of Col-0 and *mur1* mutants. Bars, 10 μ m. (d) Stomatal density and (e) frequency of 'covered' stomata on abaxial side of middle-aged leaves of 3.5-wk-old soil-grown Col-0, *mur1-1* and *mur1-2* plants. Data bars represent means \pm SD ($n = 6$ plants analyzed in three biological replicates, 2 plants per replicate). Asterisks denote statistical differences (*, $P < 0.05$; **, $P < 0.01$) to Col-0 according to one-way ANOVA followed by Dunnett's *post hoc* test.

mur1 mutants had significantly stiffer pavement cells (approximately twofold increase on average) and the same difference was observed when values obtained for guard cell walls were compared (Fig. 5b). We therefore conclude that lack of MUR1 affected mechanical properties of the leaf epidermis.

To investigate whether these properties affect stomatal movements, we assessed the closure of *mur1* stomata in response to

ABA spray by means of microscopic imaging of stomatal width : length ratio in epidermal imprints. For this, whole rosettes of Col-0, *mur1-1*, *mur1-2*, and the ABA-unresponsive *ghr1-3* mutant (Sierla *et al.*, 2018) were treated with ABA and the stomatal apertures were recorded after 45 min. This treatment led to a pronounced decrease of stomatal aperture in Col-0 while the *ghr1-3* mutant was largely unresponsive (Fig. 5c). In contrast to *ghr1-3*, the stomatal apertures of both *mur1* mutants decreased nearly to the same extent as those of Col-0 plants, indicating capability for the execution of stomatal movements in response to ABA (Fig. 5c). Analogical treatment with ABA performed 1 h before leaf excision was not sufficient to suppress the elevated water loss of *mur1* mutants (Fig. S14) indicating little correlation between the outcome of water loss assay and initial aperture of stomatal pores.

Furthermore, by microscopic real-time imaging of stomatal movements, we investigated whether *mur1* stomata close during the water loss assay. In these experiments, *ost1-3* mutant was used as a control. Before leaf excision, stomatal apertures were significantly larger in *ost1-3* while no differences between Col-0 and *mur1* mutants were observed (Fig. 5d,e). Leaf excision induced a decline, and stomata of *mur1* mutants reacted to this treatment similarly as those of Col-0 (Fig. 5d,e; Video S1). The stomatal apertures of *ost1-3* remained significantly higher than those of Col-0 and *mur1* throughout the experiment. Moreover, a large number of *ost1-3* stomata were open at the final time point of the experiment (45 min). We therefore concluded that high water loss observed in *mur1* mutants was uncoupled from stomatal movements.

Additionally, we investigated whether reduction of leaf conductance observed in *mur1* mutants during the day/night transition (Fig. S8e) can affect the outcome of water loss assay. For this, we performed water loss experiments 2 h following the onset of illumination and the night period, respectively. In these experiments, *ost1-3* and *ghr1-3* mutants were used as controls because *ost1-3* exhibits high g_s during the day and a clear decrease during the night while *ghr1-3* maintains high g_s irrespectively of the diurnal rhythm (Sierla *et al.*, 2018). In *ost1-3* mutant, values recorded at night decreased by half compared with daytime water loss, suggesting that the decrease in g_s observed during day/night transition was sufficient to limit the nocturnal water loss in this mutant. In contrast, the night-time water loss of *ghr1-3* and both *mur1* mutants was nearly as high as that recorded during the day, albeit a statistically significant difference was observed in *mur1-1* (Fig. 5f). We therefore conclude that high nocturnal water loss observed in *mur1* mutants was independent of the decrease in leaf conductance observed during the day/night transition.

Epidermal permeability, cuticle composition, and cell adhesion in *mur1* mutants

The apparent lack of correlation between the whole-rosette leaf conductance and stomatal movements as well as high nocturnal water loss suggested that *mur1* mutants lose water through non-stomatal paths. Therefore, we set out to assess their cuticular and epidermal integrity. No phenotypes related to cuticle

permeability were detected in *mur1* mutants by means of toluidine blue dye-exclusion assay (Fig. S15a); however, a moderate but consistent (albeit not always statistically significant) increase in whole-rosette ion leakage could be observed (Figs 6a, S16).

The total content of cutin monomers in *mur1* mutants was comparable to Col-0; however, differences in relative abundance of monomers could be observed (Table S2). The analysis of cuticular wax composition revealed much more pronounced differences (Fig. 6b; Table S3), with total wax levels nearly doubled in *mur1* mutants compared with Col-0. In both mutants, increased abundance of fatty alcohols, fatty acids, and sterols was observed, while the abundance of long-chain aldehydes was reduced in *mur1-2* (Fig. 6b; Table S3). Taken together, we conclude that impaired function of MUR1 had little effect on total cutin content but led to changes in cutin composition and overproduction of cuticular wax.

Additionally, we tested whether lack of GDP-L-Fuc leads to loss of epidermal cell adhesion as the water loss of the cell adhesion mutant *quasimodo2* (*qua2-1*; Mouille *et al.*, 2007) was comparable to that of *mur1* (Fig. 6c). Indeed, during observation of dark-elongated hypocotyls of *mur1* mutants we sporadically observed symptoms of loss of cell adhesion, visible as peeling of epidermal cells; however, this phenotype was not as severe as that of *qua2-1* (Fig. S17). Moreover, we found that cell adhesion mutants *qua2-1* and *qua1-1* (Bouton *et al.*, 2002) stained strongly with toluidine blue (Fig. S15b) and exhibited ion leakage much higher than that of *mur1* mutants (Fig. 6a). In *qua2*, the loss of cell adhesion requires ESMEALDA1 (ESMD1) and can be suppressed by introduction of the *esmd1-1* mutation (Verger *et al.*, 2016). We found that the water loss and ion leakage were nearly fully suppressed in *qua2-1 esmd1-1* double mutant but not in *mur1 esmd1-1* double mutants (Figs 6c, S16). Finally, during the examination of *mur1* epidermis by means of cryo-SEM we did not detect any morphological signs indicative of loss of cell adhesion that are otherwise readily visible in cell adhesion mutants (Verger *et al.*, 2018; Lorrain *et al.*, 2021; Dataset S3b,c). We therefore conclude that the lack of GDP-L-fucose had a minor effect on the adhesion of epidermal cells, and loss of epidermal cell adhesion was not the cause of elevated water loss observed in *mur1* mutants.

High water loss in boron uptake mutant

To investigate whether high water loss of *mur1* was related to the dimerization of RG-II, we grew *mur1* mutants in soil supplemented with 1 mM borate. Such treatments were previously shown to compensate for the deficiency in RG-II crosslinking (O'Neill *et al.*, 2001). We observed a significant decrease in water loss of *mur1* mutants grown in the presence of 1 mM borate compared with the control conditions (Fig. 7a). A similar trend was observed in Col-0, *slac1-4*, and *gbr1-3* mutants, albeit to a much lower extent, possibly indicating general reduction in transpiration to prevent excess B accumulation (Macho-Rivero *et al.*, 2018). To validate this finding, we utilized plants lacking the REQUIRES HIGH BORON1 (BOR1) boron transporter required for boron xylem loading (Noguchi *et al.*, 1997; Takano

et al., 2002) as the impaired uptake of boron was previously demonstrated to affect not only the dimerization of RG-II (Miwa *et al.*, 2013; Panter *et al.*, 2019) but also membrane integrity (Cakmak *et al.*, 1995; Han *et al.*, 2008). We found that a soil-grown *bor1-3* mutant (Kasai *et al.*, 2011) exhibited high water loss which could be fully reverted by supplementing the soil with 50 μ M borate, while lower concentrations (10 and 20 μ M) had less effect (Fig. 7b). The water loss of mutants impaired in fucosylation of xyloglucan (*mur2-1*; Vanzin *et al.*, 2002); arabinogalactan proteins (*fut4 fut6*; Tryfona *et al.*, 2014) and N-glycans: *fucta fuctb* (Strasser *et al.*, 2004), *fuctc-1* (Rips *et al.*, 2017) was comparable to that of Col-0 (Fig. 7c), suggesting that high water loss observed in *mur1* was not related to impaired fucosylation of these cell wall components. Collectively, our data supported the hypothesis that high water loss observed in *mur1* plants is related to a deficiency in RG-II crosslinking and/or membrane integrity.

Discussion

Synthesis of GDP-L-fucose and boron uptake are required for normal plant gas exchange

Here, we report the identification of impaired regulation of gas exchange in plants lacking MUR1 – an enzyme catalyzing the first step in *de novo* GDP-L-Fuc synthesis pathway (Bonin *et al.*, 1997). Plants lacking GDP-L-Fuc exhibited high loss of water from detached leaves (Fig. 1) and impaired decrease in leaf conductance in response to O₃, ABA, darkness, and high CO₂ concentration (Figs 3, S8, S9; Dataset S2). High water loss observed in *mur1* appears independent from canonical guard cell signaling pathways (Fig. 5a) and was also detected in plants impaired in import of GDP-L-Fuc into the Golgi apparatus (Fig. 2). Therefore, we conclude that not only synthesis but also the import of GDP-L-Fuc into the Golgi lumen is required for normal gas exchange.

The fucosylation of cell wall components is thought to occur in the Golgi apparatus (Fig. S1; Chou *et al.*, 2015; Strasser, 2016), and the majority of fucose is incorporated into the cell wall via the Golgi-derived vesicles (Anderson *et al.*, 2012). We excluded the possibility that phenotypes observed in *mur1* might be linked to impaired fucosylation of AGPs, N-linked glycans, and xyloglucan (Fig. 7c). The reversion of the *mur1* water loss phenotype by borate supplementation (Fig. 7a), and high water loss observed in *bor1-3* mutant (Fig. 7b), suggests that the phenotype was linked either directly or indirectly, to the structure and dimerization of RG-II. Recently, Panter *et al.* (2023) arrived at the same conclusions.

Depletion of GDP-L-Fuc also likely impairs protein o-fucosylation. The only characterized Arabidopsis protein o-fucosyltransferase SPINDLY (Zentella *et al.*, 2017) was shown to be required for the great majority of o-fucosylation events (Bi *et al.*, 2023). However, we did not detect high water loss in *spy* mutants (data not shown). Moreover, SPY is a nucleocytoplasmic protein while our data suggest that import of GDP-L-fucose into Golgi is required to restrict water loss (Fig. 2). Taken together,

we conclude that high water loss observed in *mur1* mutants was related to impaired RG-II crosslinking. However, based on data generated in this work, we cannot exclude additional functions of GDP-L-Fuc and boron, that could also contribute to gas exchange regulation (discussed further below).

Stomatal movements and cuticular barriers in *mur1* mutants

Our AFM data indicated that the cell walls of *mur1* guard cells and epidermal cells were significantly stiffer than that of WT

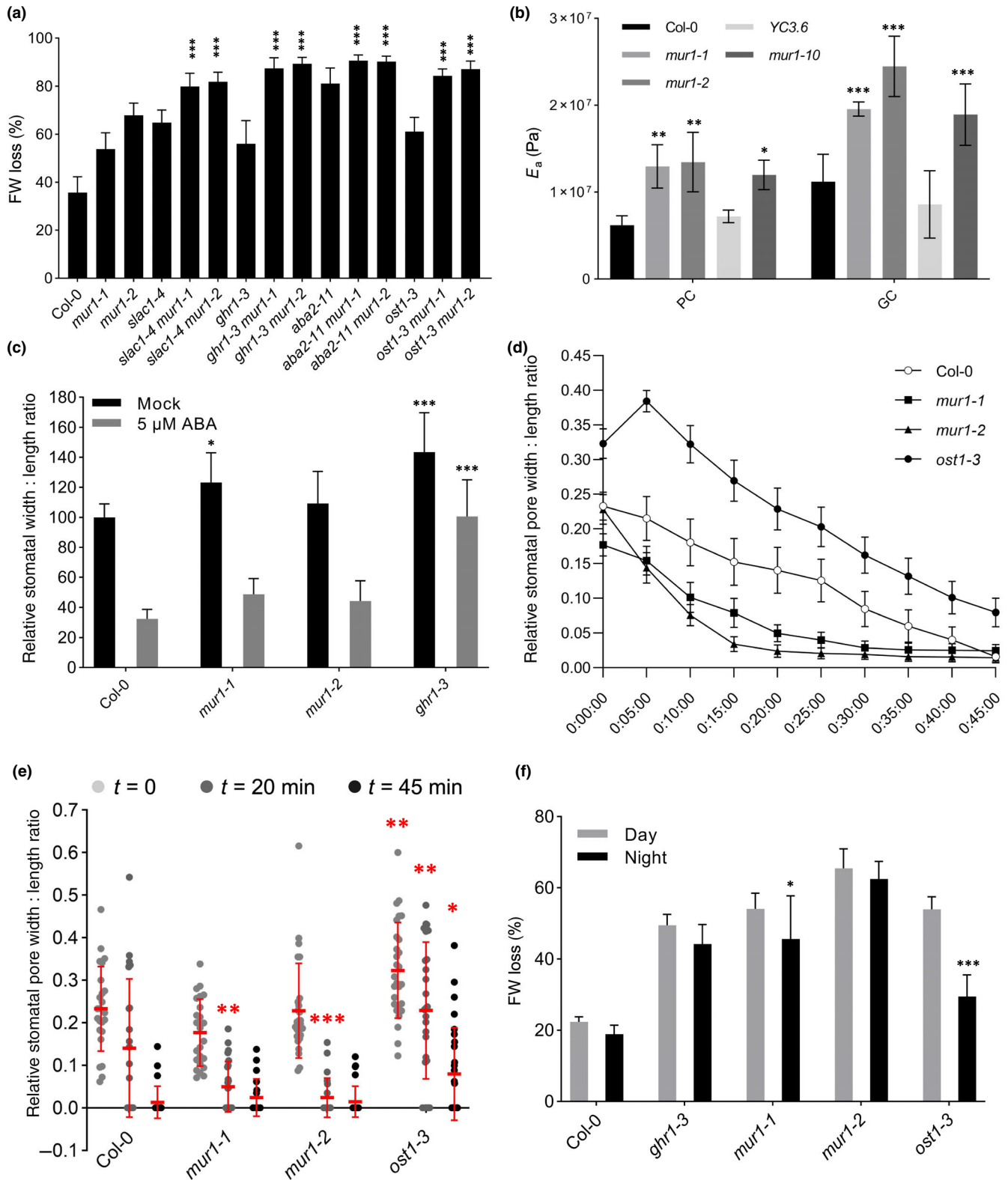


Fig. 5 Functional analysis of *mur1* stomata. (a) Leaf fresh weight loss of *Arabidopsis thaliana* double mutants obtained after crossing *slac1-4*, *ghr1-3*, *aba2-11*, and *ost1-3* with *mur1-1* and *mur1-2* recorded after 1 h. Data bars represent means \pm SD ($n = 13\text{--}16$ plants). Asterisks denote statistical differences (***, $P < 0.001$) to respective single mutant lines (*slac1-4*, *ghr1-3*, *aba2-11*, and *ost1-3*) according to one-way ANOVA followed by Sidák's *post hoc* test. Experiment was repeated three times with similar results. Results of the representative experiment are shown. (b) Average apparent Young's modulus (E_a) values derived from atomic force microscopy (AFM) scans of pavement cells (PC) and guard cells (GC) of control (Col-0, YC3.6) and *mur1 A. thaliana* plants. Bars represent means \pm SD ($n = 2\text{--}3$ plants, 2 stomata per plant). Asterisks denote statistical differences according to two-way ANOVA, followed by Tukey's *post hoc* test (*, $P < 0.05$; **, $P < 0.01$; ***, $P < 0.001$) to respective control lines (Col-0, YC3.6) observed within a cell type. (c) Normalized stomatal width : length ratio observed on epidermal imprints of abaxial side of *A. thaliana* middle-aged leaves 45 min after spray with 5 μM abscisic acid (ABA) or mock solution. Data bars represent means \pm SD, $n = 8$ plants analyzed in four biological replicates (two plants per replicate, two leaves per plant, at least 30 stomata per plant). Within each replicate, values were normalized to mock-treated Col-0. Asterisks denote statistical differences (*, $P < 0.05$; ***, $P < 0.001$) to Col-0 within each treatment according to two-way ANOVA followed by Sidák's *post hoc* test. (d) Time course of stomatal pore width : length ratios observed on abaxial side of middle-aged leaves of *Arabidopsis thaliana mur1* mutants and control lines (Col-0 and *ost1-3*) after leaf detachment. Leaves were detached at $t = 0$. Data points represent means \pm SE $n = 24\text{--}28$ stomata per genotype (six plants per genotype, typically 3–5 stomata per plant). (e) Statistical analysis of data presented in panel (d). Data points represent values recorded for individual stomata, red horizontal bars represent means \pm SE. Red asterisks (*, $P < 0.05$; **, $P < 0.01$; ***, $P < 0.001$) indicate significant differences to Col-0 within each time point according to two-way ANOVA followed by Dunnett's *post hoc* test. (f) Leaf fresh weight loss of *A. thaliana mur1* mutants and control lines (Col-0, *ost1-3* and *ghr1-3*) recorded after 2 h. Experiments were performed 2 h after the beginning (Day), or end (Night), of the light period. Data bars represent means \pm SD ($n = 6\text{--}8$ plants). Asterisks (*, $P < 0.05$; ***, $P < 0.001$) denote statistical differences (Day vs Night) within each genotype according to two-way ANOVA followed by Sidák's *post hoc* test. Experiment was repeated four times with similar results. Results of the representative experiment are shown.

plants (Fig. 5b). While mechanical properties of guard cell walls are expected to change the dynamics of stomatal movements (Jones *et al.*, 2003; Amsbury *et al.*, 2016; Rui *et al.*, 2017), our data clearly indicate that *mur1* stomata were capable of closure (Fig. 5c–e; Video S1). Similar conclusions can be drawn from studies by Zhang *et al.* (2019) and Panter *et al.* (2023) who demonstrated nearly complete closure of *mur1* stomata in response to ABA treatment. Moreover, we found that *mur1* stomatal responses to opening stimuli were not impaired (Fig. S10), suggesting that altered *mur1* cell wall mechanics does not have a profound effect on stomatal movements. Finally, we found that pretreatment with ABA or night stimulus which clearly decreased leaf conductance of *mur1* mutants (Fig. S8e) had little effect on *mur1* water loss (Figs S14, 5f). Thus, we conclude that high water loss observed in *mur1* mutants cannot be readily compared to that observed in classical stomatal mutants such as *ghr1* or *ost1* and likely has a different mechanistic origin.

Despite moderate increase in ion leakage (Fig. 6a) and changes in cutin composition (Fig. 6b; Table S2), *mur1* mutants did not exhibit elevated leaf conductance (Fig. S13) or staining with toluidine blue (Fig. S15a; Lorrai *et al.*, 2021; Panter *et al.*, 2023) that is otherwise typical for cuticular and cell adhesion mutants (Jakobson *et al.*, 2016; Fig. S15). In agreement with these data, we did not detect morphological symptoms of loss of epidermal cell adhesion in *mur1* mutants (Dataset S3) and found that the introduction of *esmd1-1* mutation into the *mur1* background did not reduce its water loss (Fig. 6c).

Loss of epidermal/cuticular barriers caused by impaired cutin deposition (Bessire *et al.*, 2007; Voisin *et al.*, 2009) or loss of epidermal cell adhesion (Lorrai *et al.*, 2021) was found to cause strong resistance to *Botrytis cinerea*. However, in the same study Lorrai *et al.* (2021) observed no increased resistance to this pathogen in *mur1* mutant, suggesting no radical changes in the permeability of epidermal/cuticular barriers. Taken together, our data suggest that gas exchange phenotypes observed in *mur1* did not

stem from general defects in cutin synthesis or epidermal cell adhesion, that is elevated g_{cuti} .

How do *mur1* mutants lose water?

Due to the limited phenotypical similarities between *mur1* and classical mutants impaired in stomatal movements, cutin synthesis or epidermal cell adhesion, *mur1* mutants cannot be clearly placed into any of these categories. The apparent lack of correlation between measured stomatal apertures and leaf conductance and transpiration (Figs 3e, 5c), leaf conductance and water loss (Figs S8e, 5f) as well as normal stomatal movements following leaf detachment (Fig. 5d,e; Video S1) suggest that *mur1* stomata are permeable to water vapor even in the closed state. This phenomenon, that is high minimal stomatal conductance, is thought to significantly contribute to g_{min} (Kerstiens, 1996; Duursma *et al.*, 2019; Machado *et al.*, 2021). High $g_{\text{s-min}}$ can be associated with higher stomatal density, imperfect closure of stomata and possibly other structural features of guard cells or mesophyll. Our data (Fig. 4a,d), combined with earlier reports (Zeng *et al.*, 2011; Panter *et al.*, 2023) indicate that the stomatal density in *mur1* mutants is not elevated. The size of stomatal complexes was somewhat elevated in *mur1* mutants (Fig. 4b; Zeng *et al.*, 2011; Panter *et al.*, 2023); however, we found that this did not significantly increase the steady-state leaf conductance or transpiration (Figs S8–S10, S13). Thus, the gas exchange profiles of *mur1* mutants might be explained by the imperfect closure of stomata that likely leads to an increase in minimal stomatal conductance.

An explanation for the elevated $g_{\text{s-min}}$ might be offered by the observation of stomatal morphology in *mur1* mutants. In agreement with earlier reports (Zeng *et al.*, 2011; Panter *et al.*, 2023), we found that *mur1* stomata exhibit a range of structural defects, most notably, altered structure of outer cuticular ledges (Figs 4, S12; Dataset S3). It is tempting to speculate that changes in

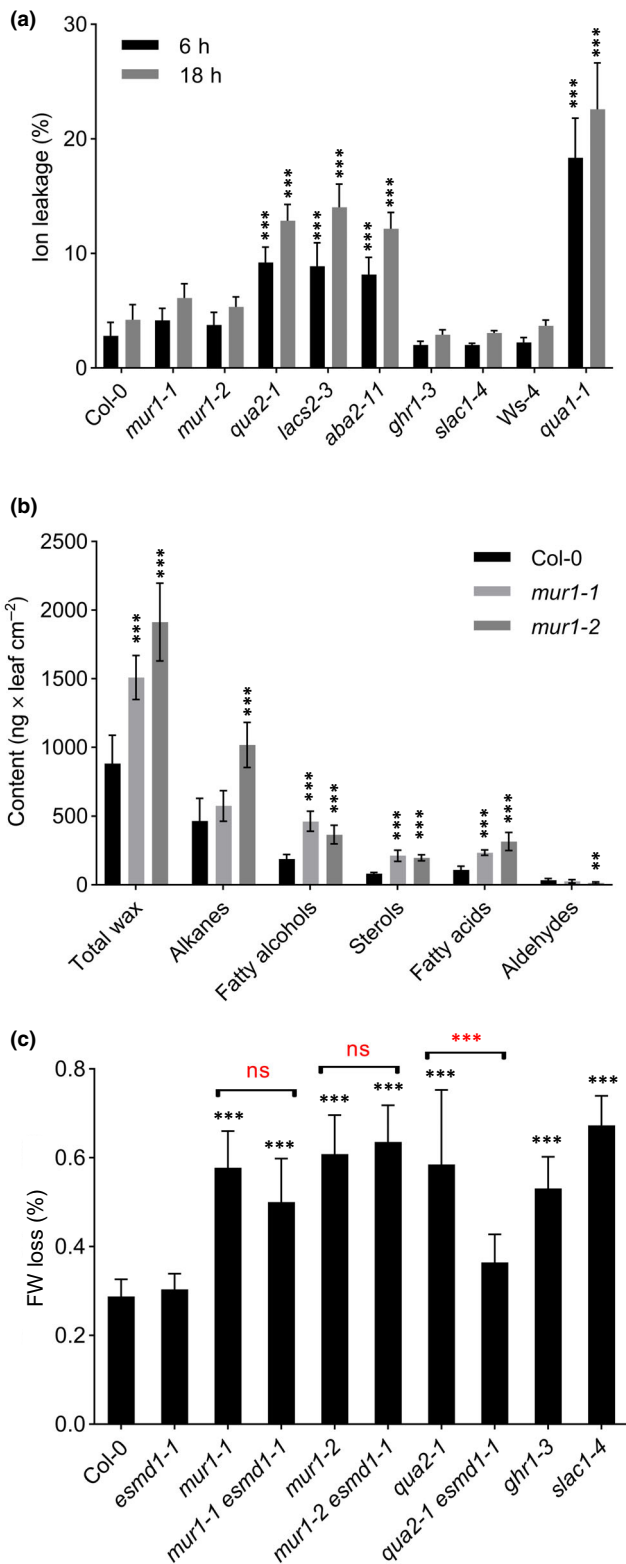


Fig. 6 Epidermal integrity in *mur1* mutants. (a) Ion leakage in 6 and 18 h expressed as % of total ion content. Data bars represent means \pm SD ($n = 5-6$ plants). Asterisks denote statistical differences according to two-way ANOVA, followed by Tukey's *post hoc* test (***, $P < 0.001$) to Col-0 observed within each time point. Experiment was repeated seven times with similar results. Results of the representative experiment are shown. (b) Analysis of wax content by GC-MS. Data bars represent means \pm SD ($n = 8$ plants) calculated based on data presented in Supporting Information Table S3. Asterisks denote statistical differences (**, $P < 0.01$; ***, $P < 0.001$) to Col-0 within each compound group, according to two-way ANOVA followed by Dunnett's *post hoc* test. (c) Leaf fresh weight loss of double mutants obtained after crossing *mur1-1*, *mur1-2* and *qua2-1* with *esmd1-1*, recorded after 2 h. Data bars represent means \pm SD ($n = 7-8$ plants). Asterisks denote statistical differences (***, $P < 0.001$; ns, not significant) to Col-0 (black) or respective single mutant lines (red), according to one-way ANOVA followed by Šidák's *post hoc* test. Experiment was repeated four times with similar results. Results of the representative experiment are shown. (a-c) Experiments performed on whole rosettes (a) or middle-aged leaves (b, c) of 3.5- (a, c) or 5-wk-old (b) soil-grown *Arabidopsis thaliana* plants.

OCLs. However, it cannot be excluded that the cuticle composition changes are a secondary effect of stress signaling (Voxeur *et al.*, 2017; Chen *et al.*, 2022). The precise function of OCLs is still poorly characterized (Hunt & Gray, 2020); however, changes in OCL structure provide little explanation for additive water loss observed in double mutants of *mur1* and guard cell signaling components (Fig. 5a).

The excision of leaves leads to a rapid decrease in leaf water potential, leading to transient increase in g_s (usually described as 'wrong way response') and initial drop in leaf temperature, which is ultimately followed by maximal stomatal closure with g_s values reaching g_{s-min} (Powles *et al.*, 2006) and increase in leaf temperature (Fig. S5). Under conditions of no water supply observed after leaf excision, the relative humidity in the substomatal cavities and mesophyll air spaces is expected to drop below saturation, ultimately triggering, and linking the evaporation rate to the active control of plasma membrane hydraulic conductivity (Wong *et al.*, 2022), while primary cell walls were proposed to influence plant-water relations over 40 yr ago (Jarvis & Slatyer, 1970) and emerge as important regulators of mesophyll conductance to CO₂ (Evans, 2021), within the mesophyll the major resistance to water vapor is attributed mostly to plasma membrane aquaporins (Wong *et al.*, 2022). Aside from controlling cell wall porosity (Fleischer *et al.*, 1999), RG-II was demonstrated to form borate-dependent linkages with plasma membrane sphingolipids in cultured *Rosa* cells (Voxeur & Fry, 2014) and boron deficiency affects membrane integrity (Cakmak *et al.*, 1995; Han *et al.*, 2008). Increased ion (Figs 6a, S16) and chlorophyll leakage (Lorrai *et al.*, 2021) observed in *mur1* mutants likely stem from the same causes. It is thus possible that elevated membrane permeability, which otherwise does not affect the steady-state leaf conductance, gains significance under conditions of severe water deficit, contributing to high water loss observed in *mur1* mutants. However, the relative contribution of stomatal morphology and membrane integrity to the observed gas exchange phenotypes awaits further investigation.

cuticle composition observed in *mur1* mutants (Fig. 6b; Tables S2, S3) might be responsible for the OCL-related phenotypes. Importantly, the same structural defects were recently identified also in boron uptake mutant (Panter *et al.*, 2023) which implies a link between uptake of boron and morphology of

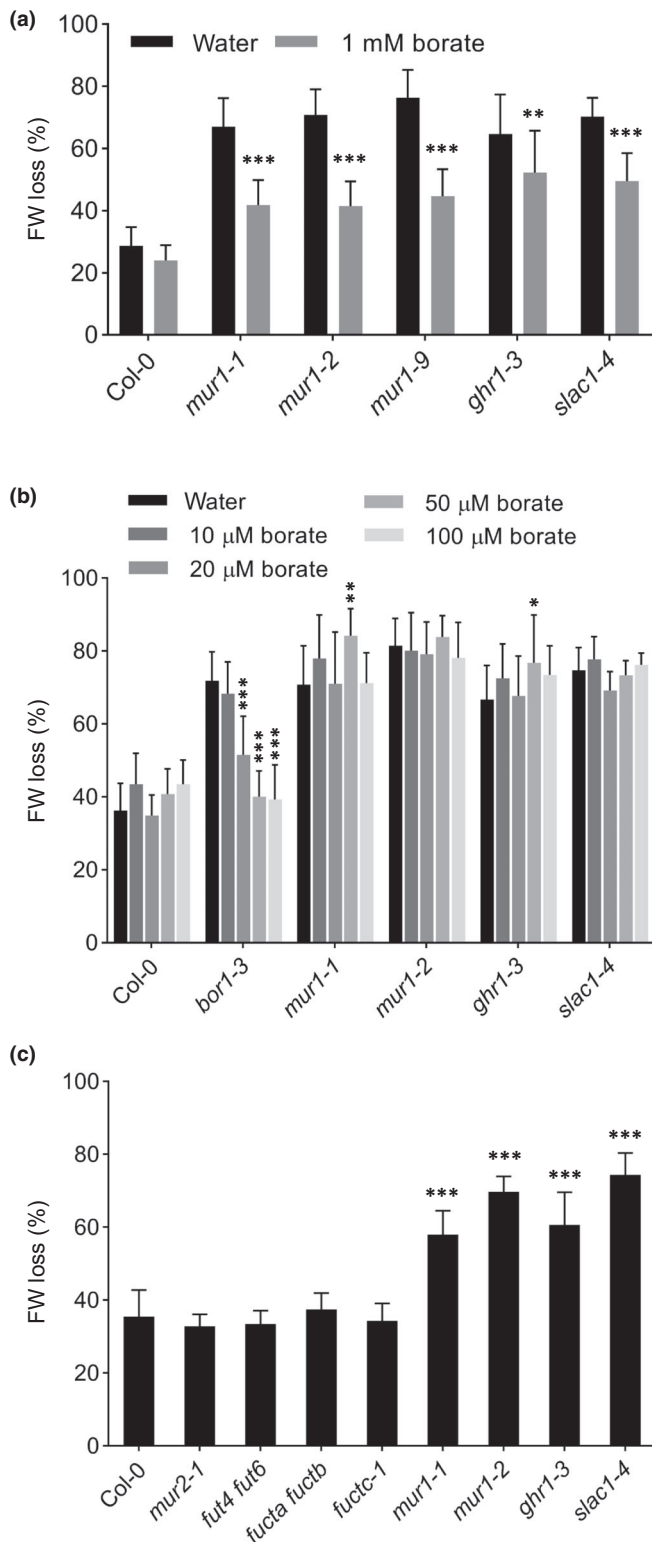


Fig. 7 Effect of borate supplementation on water loss. (a) The effect of borate supplementation on the leaf fresh weight loss of *Arabidopsis thaliana* *mur1* mutants and control lines (Col-0, *ghr1-3*, and *slac1-4*). Bars represent means \pm SD ($n = 14$ – 16 plants). Data analyzed with two-way ANOVA followed by Šidák's *post hoc* test. Asterisks denote statistical significances (**, $P < 0.01$; ***, $P < 0.001$) of treatment effect within each genotype. (b) The influence of borate supplementation on leaf fresh weight loss of *Arabidopsis thaliana* *bor1-3* mutant and control lines. Data bars represent means \pm SD ($n = 10$ – 16 plants per genotype per concentration). Asterisks denote statistical differences within each genotype, according to two-way ANOVA, followed by Tukey's *post hoc* test (*, $P < 0.05$; **, $P < 0.01$; ***, $P < 0.001$), to plants watered with tap water. (c) Leaf fresh weight loss of *A. thaliana* fucosyltransferase mutants and control lines recorded after 2 h. Data bars represent means \pm SD ($n = 10$ – 12 plants). Asterisks denote statistical differences (***, $P < 0.001$) to Col-0 according to one-way ANOVA followed by Dunnett's *post hoc* test. (a–c) Experiments were repeated five (a), three (b, c) times with similar results. Results of the representative experiments are shown.

Acknowledgements

We thank Julian Schroeder, Toshihisa Kotake, Pedro L. Rodríguez, Richard Strasser, Koh Iba, Grégory Mouille, and Paul Dupree for providing seeds of several mutants used in this study. We thank Joshua Heazlewood and Berit Ebert for providing *Agrobacterium tumefaciens* strain carrying the hpGFT1 construct, T1 seeds of hpGFT1 and corresponding EVC. Łukasz Wiczolek, Julia Palorinne, Anna Huusari, Konrad Łosiński, Jelena Odintsova, and Samuli Lundström are acknowledged for excellent technical help. Leena Grönholm and Valteri Lehtonen are acknowledged for maintaining the plant growth facilities. Personnel of the DNA sequencing and genomics laboratory are acknowledged for the technical assistance with NGS. Mervi Lindman and Lide Yao are acknowledged for assistance with electron microscopy. We gratefully acknowledge Hans Lang for an excellent technical support during the ozone fumigation experiments at the EUS. We thank Andreas Albert and the technical staff of EUS for outstanding support during the experiment. Thanks to Mikael Brosché, Kirk Overmyer, Grégory Mouille, and Teemu Hölttä for helpful comments and discussions throughout the duration of the project. This work was supported by the Research Council of Finland Centre of Excellence programs (2014–2019; 2022–2029), Research Council of Finland postdoctoral fellowships (Decision 294580, CW; 266793, TV), Research Council of Finland Research Fellowship (Decision 333703, MS), University of Helsinki 3-yr research grant (CW, MLG), EDUFI fellowship (MLG), The Ella and Georg Ehrnrooth Foundation (CW, MS), Finnish Cultural Foundation (MS), Dora Plus Programme (Contract No. 36.9-6.1/1372, OZ), Estonian Research Council (PRG433, HK; PUT311, PRG719, DY), European Regional Development Fund (Center of Excellence in Molecular Cell Engineering CEMCE, HK). The ozone exposure experiments performed at the HMGU were supported by Transnational Access program of the European Plant Phenotyping Network (EPPN, grant no. 284443) funded by the FP7 Research Infrastructures Programme of the European Union.

Competing interests

None declared.

We conclude that the abnormal gas exchange regulation observed in *mur1* is linked to altered mechanical and morphological properties of stomatal complexes likely accompanied by additional defects, for example impaired membrane integrity. In summary, our study highlights the key role of fucose metabolism and boron uptake in determining plant–water relations.

Author contributions

JK conceived the ozone-sensitivity screen; CW, TV, DY, MS, MLG, RC, NS, AJF, MXA, HK and JK designed experiments; CW, TV, DY, MS, OZ, MLG, RC, TP, NS, AL, LP, PA, AJF and MXA performed experiments and analyzed the data; JD, DE and JBW provided technological solutions for large-scale O₃ exposures; CW, DY, HK and JK wrote the manuscript with comments from all co-authors.

ORCID

Mats X. Andersson  <https://orcid.org/0000-0003-4279-6572>
 Petri Auvinen  <https://orcid.org/0000-0002-3947-4778>
 Ross Carter  <https://orcid.org/0000-0002-6251-7545>
 Jörg Durner  <https://orcid.org/0000-0003-4436-4415>
 Dieter Ernst  <https://orcid.org/0000-0003-0503-0228>
 Andrew J. Fleming  <https://orcid.org/0000-0002-9703-0745>
 Jaakko Kangasjärvi  <https://orcid.org/0000-0002-8959-1809>
 Hannes Kollist  <https://orcid.org/0000-0002-6895-3583>
 Airi Lamminmäki  <https://orcid.org/0000-0002-6133-8553>
 Marina Leal Gavarrón  <https://orcid.org/0000-0002-2879-1516>
 Lars Paulin  <https://orcid.org/0000-0003-0923-1254>
 Tuomas Puukko  <https://orcid.org/0000-0001-8452-2030>
 Maija Sierla  <https://orcid.org/0000-0002-8493-3582>
 Nina Sipari  <https://orcid.org/0000-0002-0786-2493>
 Triin Vahisalu  <https://orcid.org/0000-0001-6050-0320>
 Cezary Waszczak  <https://orcid.org/0000-0002-5978-7560>
 J. Barbro Winkler  <https://orcid.org/0000-0002-7092-9742>
 Dmitry Yarmolinsky  <https://orcid.org/0000-0002-9372-6091>
 Olena Zamora  <https://orcid.org/0000-0002-0088-0867>

Data availability

The data that support the findings of this study are available in the [Supporting Information](#).

References

- Amsbury S, Hunt L, Elhaddad N, Baillie A, Lundgren M, Verhertbruggen Y, Scheller HV, Knox JP, Fleming AJ, Gray JE. 2016. Stomatal function requires pectin de-methyl-esterification of the guard cell wall. *Current Biology* 26: 2899–2906.
- Anderson CT, Wallace IS, Somerville CR. 2012. Metabolic click-labeling with a fucose analog reveals pectin delivery, architecture, and dynamics in *Arabidopsis* cell walls. *Proceedings of the National Academy of Sciences, USA* 109: 1329–1334.
- Bar-Peled M, O'Neill MA. 2011. Plant nucleotide sugar formation, interconversion, and salvage by sugar recycling. *Annual Review of Plant Biology* 62: 127–155.
- Bessire M, Chassot C, Jacquat AC, Humphry M, Borel S, Petétot JMDC, Métraux JP, Nawrath C. 2007. A permeable cuticle in *Arabidopsis* leads to a strong resistance to *Botrytis cinerea*. *EMBO Journal* 26: 2158–2168.
- Bi Y, Shrestha R, Zhang Z, Hsu C, Reyes AV, Karunadasa S, Baker PR, Maynard JC, Liu Y, Hakimi A *et al.* 2023. SPINDLY mediates O-fucosylation of hundreds of proteins and sugar-dependent growth in *Arabidopsis*. *Plant Cell* 35: 1318–1333.
- Bonin CP, Freshour G, Hahn MG, Vanzin GF, Reiter W-D, Hahn MG. 2003. The GMD1 and GMD2 genes of *Arabidopsis* encode isoforms of GDP-D-mannose 4,6-dehydratase with cell type-specific expression patterns. *Plant Physiology* 132: 883–892.
- Bonin CP, Potter I, Vanzin GF, Reiter W-D. 1997. The MUR1 gene of *Arabidopsis thaliana* encodes an isoform of GDP-D-mannose-4,6-dehydratase, catalyzing the first step in the *de novo* synthesis of GDP-L-fucose. *Proceedings of the National Academy of Sciences, USA* 94: 2085–2090.
- Bonin CP, Reiter WD. 2000. A bifunctional epimerase-reductase acts downstream of the MUR1 gene product and completes the *de novo* synthesis of GDP-L-fucose in *Arabidopsis*. *The Plant Journal* 21: 445–454.
- Bouton S, Leboeuf E, Mouille G, Leydecker MT, Talbotec J, Granier F, Lahaye M, Höfte H, Truong HN. 2002. QUASIMODO1 encodes a putative membrane-bound glycosyltransferase required for normal pectin synthesis and cell adhesion in *Arabidopsis*. *Plant Cell* 14: 2577–2590.
- Cakmak I, Kurz H, Marschner H. 1995. Short-term effects of boron, germanium and high light intensity on membrane permeability in boron deficient leaves of sunflower. *Physiologia Plantarum* 95: 11–18.
- Carroll S, Amsbury S, Durney CH, Smith RS, Morris RJ, Gray JE, Fleming AJ. 2022. Altering arabinins increases *Arabidopsis* guard cell flexibility and stomatal opening. *Current Biology* 32: 3170–3179.
- Carter R, Woolfenden H, Baillie A, Amsbury S, Carroll S, Healcon E, Sovatzoglou S, Braybrook S, Gray JE, Hobbs J *et al.* 2017. Stomatal opening involves polar, not radial, stiffening of guard cells. *Current Biology* 27: 2974–2983.
- Chalfoun J, Majurski M, Blattner T, Bhadriraju K, Keyrouz W, Bajcsy P, Brady M. 2017. MIST: accurate and scalable microscopy image stitching tool with stage modeling and error minimization. *Scientific Reports* 7: 4988.
- Chen X, Smith SM, Shabala S, Yu M. 2022. Phytohormones in plant responses to boron deficiency and toxicity. *Journal of Experimental Botany* 74: 743–754.
- Chen Y, Li W, Turner JA, Anderson CT. 2021. PECTATE LYASE LIKE12 patterns the guard cell wall to coordinate turgor pressure and wall mechanics for proper stomatal function in *Arabidopsis*. *Plant Cell* 33: 3134–3150.
- Chou YH, Pogorelko G, Young ZT, Zobotina OA. 2015. Protein-protein interactions among xyloglucan-synthesizing enzymes and formation of Golgi-localized multiprotein complexes. *Plant & Cell Physiology* 56: 255–267.
- Duursma RA, Blackman CJ, Lopéz R, Martin-StPaul NK, Cochard H, Medlyn BE. 2019. On the minimum leaf conductance: its role in models of plant water use, and ecological and environmental controls. *New Phytologist* 221: 693–705.
- Evans JR. 2021. Mesophyll conductance: walls, membranes and spatial complexity. *New Phytologist* 229: 1864–1876.
- Fahlberg P, Buhot N, Johansson ON, Andersson MX. 2019. Involvement of lipid transfer proteins in resistance against a non-host powdery mildew in *Arabidopsis thaliana*. *Molecular Plant Pathology* 20: 69–77.
- Fleischer A, O'Neill MA, Ehwald R. 1999. The pore size of non-graminaceous plant cell walls is rapidly decreased by borate ester cross-linking of the pectic polysaccharide rhamnogalacturonan II. *Plant Physiology* 121: 829–838.
- Franks PJ, Cowan IR, Farquhar GD. 1998. A study of stomatal mechanics using the cell pressure probe. *Plant, Cell & Environment* 21: 94–100.
- González-Guzmán M, Apostolova N, Bellés JM, Barrero JM, Piqueras P, Ponce MR, Micol JL, Serrano R, Rodríguez PL. 2002. The short-chain alcohol dehydrogenase ABA2 catalyzes the conversion of xanthoxin to abscisic aldehyde. *Plant Cell* 14: 1833–1846.
- Han S, Chen LS, Jiang HX, Smith BR, Yang LT, Xie CY. 2008. Boron deficiency decreases growth and photosynthesis, and increases starch and hexoses in leaves of citrus seedlings. *Journal of Plant Physiology* 165: 1331–1341.
- Hartwig B, James GV, Konrad K, Schneeberger K, Turck F. 2012. Fast isogenic mapping-by-sequencing of ethyl methanesulfonate-induced mutant bulks. *Plant Physiology* 160: 591–600.
- Hashimoto M, Negi J, Young J, Israelsson M, Schroeder JI, Iba K. 2006. *Arabidopsis* HT1 kinase controls stomatal movements in response to CO₂. *Nature Cell Biology* 8: 391–397.
- Hedrich R. 2012. Ion channels in plants. *Physiological Reviews* 92: 1777–1811.
- Hörak H, Sierla M, Töldsepp K, Wang C, Wang YS, Nuhkat M, Valk E, Pechter P, Merilo E, Salojärvi J *et al.* 2016. A dominant mutation in the HT1 kinase uncovers roles of MAP kinases and GHR1 in CO₂-induced stomatal closure. *Plant Cell* 28: 2493–2509.

- Hunt L, Gray JE. 2020. How the stomate got his pore: very long chain fatty acids and a structural cell wall protein sculpt the guard cell outer cuticular ledge. *New Phytologist* 228: 1698–1700.
- Jakobson L, Lindgren LO, Verdier G, Laanemets K, Brosché M, Beisson F, Kollist H. 2016. BODYGUARD is required for the biosynthesis of cutin in *Arabidopsis*. *New Phytologist* 211: 614–626.
- Jarvis PG, Slatyer RO. 1970. The role of the mesophyll cell wall in leaf transpiration. *Planta* 90: 303–322.
- Jenkin S, Molina I. 2015. Isolation and compositional analysis of plant cuticle lipid polyester monomers. *Journal of Visualized Experiments* 2015: 1–10.
- Jones L, Milne JL, Ashford D, McQueen-Mason SJ. 2003. Cell wall arabinan is essential for guard cell function. *Proceedings of the National Academy of Sciences, USA* 100: 11783–11788.
- Kasai K, Takano J, Miwa K, Toyoda A, Fujiwara T. 2011. High boron-induced ubiquitination regulates vacuolar sorting of the BOR1 borate transporter in *Arabidopsis thaliana*. *The Journal of Biological Chemistry* 286: 6175–6183.
- Kerstiens G. 1996. Cuticular water permeability and its physiological significance. *Journal of Experimental Botany* 47: 1813–1832.
- Kollist T, Moldau H, Rasulov B, Oja V, Ramma H, Huve K, Jaspers P, Kangasjärvi J, Kollist H. 2007. A novel device detects a rapid ozone-induced transient stomatal closure in intact *Arabidopsis* and its absence in *abi2* mutant. *Physiologia Plantarum* 129: 796–803.
- Kotake T, Hojo S, Tajima N, Matsuoka K, Koyama T, Tsumuraya Y. 2008. A bifunctional enzyme with L-fucokinase and GDP-L-fucose pyrophosphorylase activities salvages free L-fucose in *Arabidopsis*. *The Journal of Biological Chemistry* 283: 8125–8135.
- Leonard R, Costa G, Darrambide E, Lhernould S, Fleurat-Lessard P, Carlue M, Gomord V, Faye L, Maftah A. 2002. The presence of Lewis x epitopes in *Arabidopsis thaliana* glycoconjugates depends on an active 4-fucosyltransferase gene. *Glycobiology* 12: 299–306.
- Liang Y, Basu D, Pattathil S, Xu W, Venetos A, Martin SL, Faik A, Hahn MG, Showalter AM. 2013. Biochemical and physiological characterization of *fut4* and *fut6* mutants defective in arabinogalactan-protein fucosylation in *Arabidopsis*. *Journal of Experimental Botany* 64: 5537–5551.
- Lorrai R, Francocci F, Gully K, Martens HJ, De Lorenzo G, Nawrath C, Ferrari S. 2021. Impaired cuticle functionality and robust resistance to *Botrytis cinerea* in *Arabidopsis thaliana* plants with altered homogalacturonan integrity are dependent on the class III peroxidase AtPRX71. *Frontiers in Plant Science* 12: 696955.
- Machado R, Loram-Lourenço L, Farnese FS, Alves RDFB, de Sousa LF, Silva FG, Filho SCV, Torres-Ruiz JM, Cochard H, Menezes-Silva PE. 2021. Where do leaf water leaks come from? Trade-offs underlying the variability in minimum conductance across tropical savanna species with contrasting growth strategies. *New Phytologist* 229: 1415–1430.
- Macho-Rivero MA, Herrera-Rodríguez MB, Brejcha R, Schäffner AR, Tanaka N, Fujiwara T, González-Fontes A, Camacho-Cristóbal JJ. 2018. Boron toxicity reduces water transport from root to shoot in *Arabidopsis* plants. Evidence for a reduced transpiration rate and expression of major PIP aquaporin genes. *Plant and Cell Physiology* 59: 841–849.
- Merced A, Renzaglia KS. 2018. Contrasting pectin polymers in guard cell walls of *Arabidopsis* and the hornwort *Phaeoceros* reflect physiological differences. *Annals of Botany* 123: 579–585.
- Merlot S, Leonhardt N, Fenzi F, Valon C, Costa M, Piette L, Vavasseur A, Genty B, Boivin K, Müller A *et al.* 2007. Constitutive activation of a plasma membrane H⁺-ATPase prevents abscisic acid-mediated stomatal closure. *EMBO Journal* 26: 3216–3226.
- Miwa K, Wakuta S, Takada S, Ide K, Takano J, Naito S, Omori H, Matsunaga T, Fujiwara T. 2013. Roles of BOR2, a boron exporter, in cross linking of rhamnogalacturonan II and root elongation under boron limitation in *Arabidopsis*. *Plant Physiology* 163: 1699–1709.
- Mouille G, Ralet M-C, Cavalier C, Eland C, Effroy D, Hématy K, McCartney L, Truong HN, Gaudon V, Thibault J-F *et al.* 2007. Homogalacturonan synthesis in *Arabidopsis thaliana* requires a Golgi-localized protein with a putative methyltransferase domain. *The Plant Journal* 50: 605–614.
- Nakayama KI, Maeda Y, Jigami Y. 2003. Interaction of GDP-4-keto-6-deoxymannose-3,5-epimerase-4-reductase with GDP-mannose-4,6-dehydratase stabilizes the enzyme activity for formation of GDP-fucose from GDP-mannose. *Glycobiology* 13: 673–680.
- Nieves-Cordones M, Azeem F, Long Y, Boeglin M, Duby G, Mouline K, Hosi E, Vavasseur A, Chérel I, Simonneau T *et al.* 2022. Non-autonomous stomatal control by pavement cell turgor via the K⁺ channel subunit AtKC1. *Plant Cell* 34: 2019–2037.
- Noguchi K, Yasumori M, Imai T, Naito S, Matsunaga T, Oda H, Hayashi H, Chino M, Fujiwara T. 1997. *bor1-1*, an *Arabidopsis thaliana* mutant that requires a high level of boron. *Plant Physiology* 115: 901–906.
- O'Neill MA, Eberhard S, Albersheim P, Darvill AG. 2001. Requirement of borate cross-linking of cell wall rhamnogalacturonan II for *Arabidopsis* growth. *Science* 294: 846–849.
- Overmyer K, Tuominen H, Kettunen R, Betz C, Langebartels C, Sandermann H, Kangasjärvi J, Kangasjärvi J. 2000. Ozone-sensitive *Arabidopsis red1* mutant reveals opposite roles for ethylene and jasmonate signaling pathways in regulating superoxide-dependent cell death. *Plant Cell* 12: 1849–1862.
- Pabst M, Fischl RM, Brecker L, Morelle W, Fauland A, Köfeler H, Altmann F, Léonard R. 2013. Rhamnogalacturonan II structure shows variation in the side chains monosaccharide composition and methylation status within and across different plant species. *The Plant Journal* 76: 61–72.
- Panter PE, Kent O, Dale M, Smith SJ, Skipsey M, Thorlby G, Cummins I, Ramsay N, Begum RA, Sanhueza D *et al.* 2019. MUR1-mediated cell-wall fucosylation is required for freezing tolerance in *Arabidopsis thaliana*. *New Phytologist* 224: 1518–1531.
- Panter PE, Seifert J, Dale M, Pridgeon AJ, Hulme R, Ramsay N, Contera S, Knight H. 2023. Cell-wall fucosylation in *Arabidopsis* influences control of leaf water loss and alters stomatal development and mechanical properties. *Journal of Experimental Botany* 74: 2680–2691.
- Pei D, Hua D, Deng J, Wang Z, Song C, Wang Y, Wang Y, Qi J, Kollist H, Yang S *et al.* 2022. Phosphorylation of the plasma membrane H⁺-ATPase AHA2 by BAK1 is required for ABA-induced stomatal closure in *Arabidopsis*. *Plant Cell* 34: 2708–2729.
- Perrin RM, DeRocher AE, Bar-Peled M, Zeng W, Norambuena L, Orellana A, Raikhel NV, Keegstra K. 1999. Xyloglucan fucosyltransferase, an enzyme involved in plant cell wall biosynthesis. *Science* 284: 1976–1979.
- Powles JE, Buckley TN, Nicotra AB, Farquhar GD. 2006. Dynamics of stomatal water relations following leaf excision. *Plant, Cell & Environment* 29: 981–992.
- Rautengarten C, Ebert B, Liu L, Stonebloom S, Smith-Moritz AM, Pauly M, Orellana A, Scheller HV, Heazlewood JL. 2016. The *Arabidopsis* Golgi-localized GDP-L-fucose transporter is required for plant development. *Nature Communications* 7: 12119.
- Reiter W-D, Chapple CCS, Somerville CR. 1993. Altered growth and cell walls in a fucose-deficient mutant of *Arabidopsis*. *Science* 261: 1032–1035.
- Rhomberg S, Fuchsluger C, Rendić D, Paschinger K, Jantsch V, Kosma P, Wilson IBH. 2006. Reconstitution *in vitro* of the GDP-fucose biosynthetic pathways of *Caenorhabditis elegans* and *Drosophila melanogaster*. *The FEBS Journal* 273: 2244–2256.
- Rips S, Frank M, Elting A, Offenborn JN, von Schaewen A. 2017. Golgi α 1,4-fucosyltransferase of *Arabidopsis thaliana* partially localizes at the nuclear envelope. *Traffic* 18: 646–657.
- Rui Y, Xiao C, Yi H, Kandemir B, Wang JZ, Puri VM, Anderson CT. 2017. POLYGALACTURONASE INVOLVED IN EXPANSION3 functions in seedling development, rosette growth, and stomatal dynamics in *Arabidopsis thaliana*. *Plant Cell* 29: 2413–2432.
- Schindelin J, Arganda-Carreras I, Frise E, Kaynig V, Longair M, Pietzsch T, Preibisch S, Rueden C, Saalfeld S, Schmid B *et al.* 2012. Fiji: an open-source platform for biological-image analysis. *Nature Methods* 9: 676–682.
- Shtein I, Shelef Y, Marom Z, Zelinger E, Schwartz A, Popper ZA, Bar-On B, Harpaz-Saad S. 2017. Stomatal cell wall composition: distinctive structural patterns associated with different phylogenetic groups. *Annals of Botany* 119: 1021–1033.
- Sierla M, Hörák H, Overmyer K, Waszczak C, Yarmolinsky D, Maierhofer T, Vainonen JP, Salojärvi J, Denessiouk K, Laanemets K *et al.* 2018. The receptor-like pseudokinase GHR1 is required for stomatal closure. *Plant Cell* 30: 2813–2837.
- Sierla M, Waszczak C, Vahisalu T, Kangasjärvi J. 2016. Reactive oxygen species in the regulation of stomatal movements. *Plant Physiology* 171: 1569–1580.

- Strasser R. 2016. Plant protein glycosylation. *Glycobiology* 26: 926–939.
- Strasser R, Altmann F, Mach L, Glössl J, Steinkellner H. 2004. Generation of *Arabidopsis thaliana* plants with complex N-glycans lacking β 1,2-linked xylose and core α 1,3-linked fucose. *FEBS Letters* 561: 132–136.
- Sun H, Schneeberger K. 2015. SHOREMAP v3.0: fast and accurate identification of causal mutations from forward genetic screens. *Methods in Molecular Biology* 1284: 381–395.
- Takahashi Y, Bosmans KC, Hsu PK, Paul K, Seitz C, Yeh CY, Wang YS, Yarmolinsky D, Sierla M, Vahisalu T *et al.* 2022. Stomatal CO₂/bicarbonate sensor consists of two interacting protein kinases, Raf-like HT1 and non-kinase-activity requiring MPK12/MPK4. *Science Advances* 8: eabq6161.
- Takano J, Noguchi K, Yasumori M, Kobayashi M, Gajdos Z, Miwa K, Hayashi H, Yoneyama T, Fujiwara T. 2002. *Arabidopsis* boron transporter for xylem loading. *Nature* 420: 337–340.
- Tanaka T, Tanaka H, Machida C, Watanabe M, Machida Y. 2004. A new method for rapid visualization of defects in leaf cuticle reveals five intrinsic patterns of surface defects in *Arabidopsis*. *The Plant Journal* 37: 139–146.
- Tryfona T, Theys TE, Wagner T, Stott K, Keegstra K, Dupree P. 2014. Characterisation of FUT4 and FUT6 α -(1→2)-fucosyltransferases reveals that absence of root arabinogalactan fucosylation increases *Arabidopsis* root growth salt sensitivity. *PLoS ONE* 9: e93291.
- Vahisalu T, Kollist H, Wang Y-F, Nishimura N, Chan W-Y, Valerio G, Lamminmäki A, Brosché M, Moldau H, Desikan R *et al.* 2008. SLAC1 is required for plant guard cell S-type anion channel function in stomatal signalling. *Nature* 452: 487–491.
- Vahisalu T, Puzörjova I, Brosché M, Valk E, Lepiku M, Moldau H, Pechter P, Wang Y-S, Lindgren O, Salojärvi J *et al.* 2010. Ozone-triggered rapid stomatal response involves the production of reactive oxygen species, and is controlled by SLAC1 and OST1. *The Plant Journal* 62: 442–453.
- Van Hengel AJ, Roberts K. 2002. Fucosylated arabinogalactan-proteins are required for full root cell elongation in *Arabidopsis*. *The Plant Journal* 32: 105–113.
- Vanzin GF, Madson M, Carpita NC, Raikhel NV, Keegstra K, Reiter WD. 2002. The *mur2* mutant of *Arabidopsis thaliana* lacks fucosylated xyloglucan because of a lesion in fucosyltransferase AtFUT1. *Proceedings of the National Academy of Sciences, USA* 99: 3340–3345.
- Verger S, Chabout S, Gineau E, Mouille G. 2016. Cell adhesion in plants is under the control of putative O-fucosyltransferases. *Development* 143: 2536–2540.
- Verger S, Long Y, Boudaoud A, Hamant O. 2018. A tension-adhesion feedback loop in plant epidermis. *eLife* 7: e34460.
- Voisin D, Nawrath C, Kurdyukov S, Franke RB, Reina-Pinto JJ, Efreanova N, Will I, Schreiber L, Yephremov A. 2009. Dissection of the complex phenotype in cuticular mutants of *Arabidopsis* reveals a role of SERRATE as a mediator. *PLoS Genetics* 5: e1000703.
- Voxeur A, Fry SC. 2014. Glycosylinositol phosphorylceramides from *Rosa* cell cultures are boron-bridged in the plasma membrane and form complexes with rhamnogalacturonan II. *The Plant Journal* 79: 139–149.
- Voxeur A, Soubigou-Taconnat L, Legée F, Sakai K, Antelme S, Durand-Tardif M, Lapierre C, Sibout R. 2017. Altered lignification in *mur1-1* a mutant deficient in GDP-L-fucose synthesis with reduced RG-II cross linking. *PLoS ONE* 12: e0184820.
- Wong SC, Canny MJ, Holloway-Phillips M, Stuart-Williams H, Cernusak LA, Márquez DA, Farquhar GD. 2022. Humidity gradients in the air spaces of leaves. *Nature Plants* 8: 971–978.
- Woolfenden HC, Baillie AL, Gray JE, Hobbs JK, Morris RJ, Fleming AJ. 2018. Models and mechanisms of stomatal mechanics. *Trends in Plant Science* 23: 822–832.
- Woolfenden HC, Bourdais G, Kopischke M, Miedes E, Molina A, Robatzek S, Morris RJ. 2017. A computational approach for inferring the cell wall properties that govern guard cell dynamics. *The Plant Journal* 92: 5–18.
- Wu Y, Williams M, Bernard S, Driouch A, Showalter AM, Faik A. 2010. Functional identification of two nonredundant *Arabidopsis* α (1,2) fucosyltransferases specific to arabinogalactan proteins. *The Journal of Biological Chemistry* 285: 13638–13645.
- Xu E, Vaahera L, Brosché M. 2015. Roles of defense hormones in the regulation of ozone-induced changes in gene expression and cell death. *Molecular Plant* 8: 1776–1794.
- Yamauchi S, Takemiya A, Sakamoto T, Kurata T, Tsutsumi T, Kinoshita T, Shimazaki K. 2016. The plasma membrane H⁺-ATPase AHA1 plays a major role in stomatal opening in response to blue light. *Plant Physiology* 171: 2731–2743.
- Yang Y, Costa A, Leonhardt N, Siegel RS, Schroeder JI. 2008. Isolation of a strong *Arabidopsis* guard cell promoter and its potential as a research tool. *Plant Methods* 4: 6.
- Yi H, Chen Y, Wang JZ, Puri VM, Anderson CT. 2019. The stomatal flexoskeleton: how the biomechanics of guard cell walls animate an elastic pressure vessel. *Journal of Experimental Botany* 70: 3561–3571.
- Yoshida R, Hobo T, Ichimura K, Mizoguchi T, Takahashi F, Aronso J, Ecker JR, Shinozaki K. 2002. ABA-activated SnRK2 protein kinase is required for dehydration stress signaling in *Arabidopsis*. *Plant & Cell Physiology* 43: 1473–1483.
- Zablacki E, York WS, Pauly M, Hantus S, Reiter W-D, Chapple CCS, Albersheim P, Darvill A. 1996. Substitution of L-fucose by L-galactose in cell walls of *Arabidopsis mur1*. *Science* 272: 1808–1810.
- Zeng W, Brutus A, Kremer JM, Withers JC, Gao X, Da Jones AD, He SY. 2011. A genetic screen reveals *Arabidopsis* stomatal and/or apoplastic defenses against *Pseudomonas syringae* pv. *tomato* DC3000. *PLoS Pathogens* 7: e1002291.
- Zentella R, Sui N, Barnhill B, Hsieh W-P, Hu J, Shabanowitz J, Boyce M, Olszewski NE, Zhou P, Hunt DF *et al.* 2017. The *Arabidopsis* O-fucosyltransferase SPINDLY activates nuclear growth repressor DELLA. *Nature Chemical Biology* 13: 479–485.
- Zhang L, Paasch BC, Chen J, Day B, He SY. 2019. An important role of L-fucose biosynthesis and protein fucosylation genes in *Arabidopsis* immunity. *New Phytologist* 222: 981–994.

Supporting Information

Additional Supporting Information may be found online in the Supporting Information section at the end of the article.

Dataset S1 List of *Arabidopsis thaliana* lines and primers used in this study.

Dataset S2 Kinetics of changes in leaf conductance recorded for *Arabidopsis thaliana mur1* mutants and control lines (Col-0 and *ghr1-3*) following exposure to stomata-closing stimuli.

Dataset S3 Cryo-SEM images of abaxial and adaxial epidermis of *Arabidopsis thaliana mur1* mutants.

Fig. S1 Synthesis and metabolism of GDP-L-fucose in *Arabidopsis thaliana*.

Fig. S2 Characterization of *T7-9* gas exchange dynamics following exposure to stomata-closing stimuli.

Fig. S3 Relative *MURI* transcript level in Col-0 and *mur1-9* plants.

Fig. S4 Water loss-based screen of *Arabidopsis thaliana* T-DNA insertion mutants of *T7-9* candidate genes.

Fig. S5 Leaf temperature changes recorded in *Arabidopsis thaliana mur1* mutants and control lines (Col-0 and *ghr1-3*) during the water loss experiment.

Fig. S6 Water loss of mutants impaired in L-Fuc salvage pathway.

Fig. S7 Phenotypical analysis of *Arabidopsis thaliana* hpGFT1 T1 plants.

Fig. S8 Leaf conductance responses of *Arabidopsis thaliana mur1* mutants to stomata-closing stimuli.

Fig. S9 Transpiration responses of *Arabidopsis thaliana mur1* mutants to stomata-closing stimuli.

Fig. S10 Responses of *Arabidopsis thaliana mur1* mutants to stomata-opening stimuli.

Fig. S11 Measurement of minimal leaf conductance of *mur1* mutants.

Fig. S12 Frequency and phenotypes of atypical stomata observed in cotyledons of *Arabidopsis thaliana mur1* mutants.

Fig. S13 Daytime leaf conductance of *mur1* mutants.

Fig. S14 Effect of ABA pretreatment on water loss of *mur1* mutants.

Fig. S15 Cuticle permeability of *mur1* and cell adhesion mutants.

Fig. S16 Effect of *esmd1-1* mutation on ion leakage of *qua2-1* and *mur1* mutants.

Fig. S17 Phenotyping of cell adhesion in elongated hypocotyls of *qua2-1* and *mur1* mutants.

Methods S1 Detailed description of methods used in this study.

Table S1 High-frequency single nucleotide polymorphisms identified in BC1F2 mapping population of *Arabidopsis thaliana T7-9* mutant.

Table S2 GC–MS analysis of absolute and relative abundance of cutin monomers in *Arabidopsis thaliana mur1* mutants.

Table S3 GC–MS analysis of cuticular wax composition in *mur1* mutants.

Video S1 Stomatal movements of *Arabidopsis thaliana mur1* mutants and control lines (Col-0 and *ost1-3*) observed after leaf detachment. Leaves were detached from the rosette at $t = 5$ min ('Excision'), and the imaging was continued for *c.* 40 min.

Please note: Wiley is not responsible for the content or functionality of any Supporting Information supplied by the authors. Any queries (other than missing material) should be directed to the *New Phytologist* Central Office.